A 3D cell-centered ADER MOOD Finite Volume method for solving updated Lagrangian hydrodynamics and hyperelasticity on unstructured grids

R. Loubère
W. Boscheri P.-H. Maire

raphael.loubere@math.u-bordeaux.fr

Université de Bordeaux, Institut de Mathématiques de Bordeaux (IMB), UMR-5251

February 2nd 2022 - Strasbourg (IRMA)

Outline

Outline

Lagrangian methods/schemes

$$\frac{D}{Dt}() = \frac{\partial}{\partial t}() + \bar{\mathbf{v}}\,\nabla()$$

[1] J. Von Neumann, R. D. Richtmyer. A method for the numerical calculation of hydrodynamic shocks.*J. Applied Physics* 21 (1950) 232-237.

Advantages

- availability of trajectory information;
- less numerical diffusion, no mass flux btw cells;
- mesh moves with fluid velocity;
- material interfaces are precisely located and identified.

Lagrangian methods/schemes

$$\frac{D}{Dt}() = \frac{\partial}{\partial t}() + \overline{\mathbf{v}}\,\nabla()$$

[1] J. Von Neumann, R. D. Richtmyer. A method for the numerical calculation of hydrodynamic shocks.*J. Applied Physics* 21 (1950) 232-237.

Advantages

- availability of trajectory information;
- less numerical diffusion, no mass flux btw cells;
- mesh moves with fluid velocity;
- material interfaces are precisely located and identified.

Drawbacks

- high computational cost, update mesh at each Δt;
- mesh distortion, cell integrity, $\Delta t \to 0$.

Lagrangian methods (brief overview)

Cell-centered finite volume schemes for hydrodynamics

[1] C.D. Munz. On Godunov-type schemes for Lagrangian gas dynamics.
SIAM Journal on Numerical Analysis 31 (1994) 17-42.

[2] B. Després, C. Mazeran. Symmetrization of Lagrangian gas dynamic in dimension two and multimdimensional solvers.
C.R. Mecanique 331 (2003) 475-480.

[3] B. Després, C. Mazeran. Lagrangian gas dynamics in two dimensions and Lagrangian systems.
ARMA 178 (2005) 327-372.

[4] P.H. Maire. A high-order cell-centered Lagrangian scheme for two-dimensional compressible fluid flows on unstructured meshes.
J. Comput. Phys. 228 (2009) 2391-2425.

[5] P.-H. Maire, R. Abgrall, J. Breil, J. Ovadia. A cell-centered Lagrangian scheme for two-dimensional compressible flow problems.
SIAM SISC 29 (2007) 1781-1824.

Lagrangian methods (brief overview)

Finite element schemes for solid mechanics

[1] D. P. Flanagan, T. Belytschko. A uniform strain hexahedron and quadrilateral with orthogonal hourglass control.
IJNME 17 (1981) 679-706.

[2] G.L. Goudreau, J.O. Hallquist. Recent developments in large-scale finite element Lagrangian hydrocode technology.
CMAME 33 (1982) 725-757.

[3] G. Scovazzi, B. Carnes, X. Zeng, S. Rossi. A simple, stable, and accurate linear tetrahedral finite element for transient, nearly, and fully incompressible solid dynamics: a dynamic variational multiscale approach.
IJNME 106 (2016) 799-839.

Lagrangian methods (brief overview)

Finite volume schemes for solid mechanics

[1] J.A. Trangenstein and P. Colella. A higher-order Godunov method for modeling finite deformation in elastic-plastic solids.
Communications on Pure and Applied Mathematics 44 (1991) 41-100.

[2] G. Kluth, B. Després. Discretization of hyperelasticity on unstructured mesh with a cell-centered Lagrangian scheme.
JCP 229 (2010) 9092-9118.

[3] J. Bonet, A. J. Gil, C. Hean Lee, M. Aguirre, R. Ortigosa. A first order hyperbolic framework for large strain computational solid dynamics. part I: Total Lagrangian isothermal elasticity.
CMAME 283 (2015) 689-732.

[4] A. J. Gil, C. Hean Lee, J. Bonet, and R. Ortigosa. A first order hyperbolic framework for large strain computational solid dynamics. part II: Total Lagrangian compressible, nearly incompressible and truly incompressible elasticity.
CMAME 300 (2016) 146-181.

Outline

Updated Lagrangian framework

Lagrange-Euler mapping $\Phi : \boldsymbol{X} \longmapsto \boldsymbol{x} = \Phi(\boldsymbol{X}, t)$

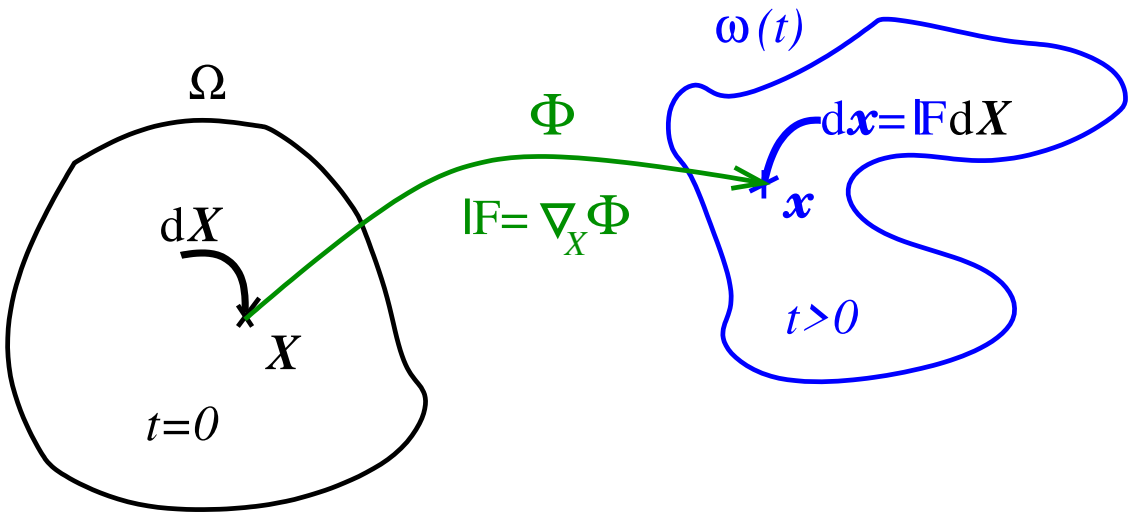

Lagrange-Euler mapping Φ relating a material Lagrangian point $\boldsymbol{X}$ at $t = 0$ and a spatial Eulerian one $\boldsymbol{x}$ at $t > 0$.

$\Omega \longrightarrow \omega(t)$	Computational domains
$\mathbb{F}(\boldsymbol{X}, t) = \nabla_X \Phi(\boldsymbol{X}, t)$	Deformation gradient
$J(\boldsymbol{X}, t) = \det(\mathbb{F}(\boldsymbol{X}, t))$	Determinant of $\mathbb{F}$
$\mathbb{F}(\boldsymbol{X}, t = 0) = \mathbb{I}_d,\ J(\boldsymbol{X}, t = 0) = 1$	Continuity $J(\boldsymbol{X}, t) > 0$

Updated Lagrangian framework

Lagrangian/Eulerian expressions

$G(\boldsymbol{X}, t)$: Lagrangian representation and $g(\boldsymbol{x}, t)$ the Eulerian one of the same physical quantity, then

$$g(\boldsymbol{x}, t) = G\left(\boldsymbol{\Phi}^{-1}(\boldsymbol{x}, t), t\right) \quad \text{and} \quad G(\boldsymbol{X}, t) = g\left(\boldsymbol{\Phi}(\boldsymbol{X}, t), t\right).$$

Time differentiation

Holding $\boldsymbol{X}$ fixed, the kinematic velocity is

$$\boldsymbol{v}(\boldsymbol{X}, t) = \frac{\partial \boldsymbol{\Phi}}{\partial t}|_{\boldsymbol{X}}(\boldsymbol{X}, t).$$

The Lagrangian time derivative is the material time derivative

$$\frac{\mathrm{d}g}{\mathrm{d}t}(\boldsymbol{x}, t) = \frac{\partial g}{\partial t}(\boldsymbol{x}, t) + \boldsymbol{v} \cdot \nabla_x g.$$

Updated Lagrangian framework

Measures of deformation

The stretching of an infinitesimal fiber $\mathrm{d}\boldsymbol{X}$ maps into $\mathrm{d}\boldsymbol{x} = \mathbb{F}\mathrm{d}\boldsymbol{X}$.

Right Cauchy-Green tensor: $\mathbb{C} = \mathbb{F}^t\mathbb{F}$

$$\mathrm{d}\boldsymbol{x} \cdot \mathrm{d}\boldsymbol{x} - \mathrm{d}\boldsymbol{X} \cdot \mathrm{d}\boldsymbol{X} = (\mathbb{C} - \mathbb{I}_\mathsf{d})\mathrm{d}\boldsymbol{x} \cdot \mathrm{d}\boldsymbol{x}.$$

Left Cauchy-Green tensor: $\mathbb{B} = \mathbb{F}\mathbb{F}^t$

$$\mathrm{d}\boldsymbol{x} \cdot \mathrm{d}\boldsymbol{x} - \mathrm{d}\boldsymbol{X} \cdot \mathrm{d}\boldsymbol{X} = (\mathbb{I}_\mathsf{d} - \mathbb{B}^{-1})\mathrm{d}\boldsymbol{X} \cdot \mathrm{d}\boldsymbol{X}.$$

Remarks

$\mathbb{B}$ and $\mathbb{C}$ are symmetric positive definite and share the same eigenvalues.
For rigid rotation they collapse to $\mathbb{I}_\mathsf{d}$.

Geometric Conservation Law (GCL)

Time differentiation of $\mathbb{F} = \nabla_X \mathbf{\Phi}$ (deformation gradient) leads to the GCL.

Total Lagrangian formulation

$$\frac{\partial \mathbb{F}}{\partial t} - \nabla_X \boldsymbol{v} = 0, \qquad \boldsymbol{v} = \frac{\partial \mathbf{\Phi}}{\partial t}.$$

Curl compatibility constraint:

$$\nabla_X \times \mathbb{F} = \mathbf{0} \qquad (1)$$

ensures $\mathbb{F}$ = gradient of a mapping.

Updated Lagrangian formulation

$$\frac{\mathrm{d}\mathbb{F}}{\mathrm{d}t} - \mathbb{L}\mathbb{F} = 0, \qquad \mathbb{L} = \nabla_x \boldsymbol{v}.$$

Time rate of change of $\mathbb{B} = \mathbb{F}\mathbb{F}^t$:

$$\frac{\mathrm{d}\mathbb{B}}{\mathrm{d}t} = \frac{\mathrm{d}\mathbb{F}}{\mathrm{d}t}\mathbb{F}^t + \mathbb{F}\frac{\mathrm{d}\mathbb{F}^t}{\mathrm{d}t} \Rightarrow \frac{\mathrm{d}\mathbb{B}}{\mathrm{d}t} - \mathbb{L}\mathbb{B} - \mathbb{B}\mathbb{L}^t = 0$$

Remarks

- (1) is an involution constraint for the GCL. True at $t = 0 \Rightarrow$ true $\forall t$.
- Discrete satisfaction of (1) is a key point for any total Lagrangian scheme.
- Updated Lagrangian equation for Jacobian yields

$$\frac{\mathrm{d}J}{\mathrm{d}t} - J\mathrm{tr}(\mathbb{L}) = 0 \Longrightarrow \frac{\mathrm{d}J}{\mathrm{d}t} - J\nabla_x \cdot \boldsymbol{v} = 0$$

Governing equations

Lagrangian conservation laws

$$\rho \frac{\mathrm{d}\tau}{\mathrm{d}t} - \nabla \cdot \boldsymbol{v} = 0,$$
$$\rho \frac{\mathrm{d}\boldsymbol{v}}{\mathrm{d}t} - \nabla \cdot \mathbb{T} = \boldsymbol{0},$$
$$\rho \frac{\mathrm{d}e}{\mathrm{d}t} - \nabla \cdot (\mathbb{T}\boldsymbol{v}) = 0,$$
$$\frac{\mathrm{d}\boldsymbol{x}}{\mathrm{d}t} = \boldsymbol{v}(\boldsymbol{x}(t), t),$$

$\mathrm{d}/\mathrm{d}t$	$\rightarrow$	material derivative
$\tau = \frac{1}{\rho} > 0$	$\rightarrow$	specific vol., mass density
$\boldsymbol{v}$	$\rightarrow$	fluid velocity
$\mathbb{T}$	$\rightarrow$	sym. Cauchy stress tensor
$e = \varepsilon + \frac{1}{2}\boldsymbol{v}^2$	$\rightarrow$	specific total energy
$\varepsilon > 0$	$\rightarrow$	specific internal energy
$\boldsymbol{x}(0) = \boldsymbol{X}$		

Closure law – Constitutive law for $\mathbb{T}$

Law expressing the Cauchy stress tensor $\mathbb{T}$ in terms of deformation and a thermodynamic variable.

Constitutive law for **gas-dynamics**

For gas-dynamics we consider

$$\mathbb{T} \equiv \mathbb{T}(\rho, \varepsilon) = -p(\rho, \varepsilon)\mathbb{I}_{\mathbf{d}},$$

with p the so-called pressure given by an Equation-Of-State (EOS) which depends on the considered 'material'

Equation of state (EOS)

- Perfect gas: Mono-atomic $\gamma = 5/3$, Diatomic $\gamma = 7/5$, Ammonia $\gamma = 1.32$

  $$p = (\gamma - 1)\rho\varepsilon, \qquad \gamma = \frac{C_P}{C_V} > 1 \qquad \text{material-dependent parameter}$$

- Stiffened gas:

  $$p = (\gamma - 1)\rho\varepsilon - \gamma\Pi_\infty, \quad \gamma = \frac{C_P}{C_V} > 1, \Pi_\infty \text{ material-dependent param.}$$

- Mie-Grunüneisen...

Constitutive law for **isotropic materials** ($\mathbb{TB} = \mathbb{BT}$)

Free energy potential: $\Psi \equiv \Psi(\mathbb{B}, \theta)$

Introduce free energy:

$$\Psi = \varepsilon - \theta\eta \equiv \Psi\left(I_1(\mathbb{B}), I_2(\mathbb{B}), I_3(\mathbb{B}), \theta\right),$$

thanks to Theorem of representation of isotropic scalar function, where $\theta > 0$, η are the absolute temperature and specific entropy, with I_k are the principal invariant[a]. of $\mathbb{B}$

[a] $I_1(\mathbb{B}) = \mathrm{tr}(\mathbb{B}), \quad I_2(\mathbb{B})) = \frac{1}{2}\left[\mathrm{tr}^2(\mathbb{B}) - \mathrm{tr}(\mathbb{B}^2)\right], \quad I_3(\mathbb{B}) = \det(\mathbb{B})$

Cauchy stress tensor: $\mathbb{T}(\mathbb{B}, \theta) = 2\rho\left(\frac{\partial\Psi}{\partial\mathbb{B}}\right)_\theta \mathbb{B}$

Differentiation of Ψ w.r.t. $\mathbb{B}$ leads to
$\left(\frac{\partial\Psi}{\partial\mathbb{B}}\right)_\theta = \left(\frac{\partial\Psi}{\partial I_1}\right)_\theta \mathbb{I}_\mathrm{d} + \left(\frac{\partial\Psi}{\partial I_2}\right)_\theta (I_1\mathbb{I}_\mathrm{d} - \mathbb{B}) + \left(\frac{\partial\Psi}{\partial I_3}\right)_\theta I_3\mathbb{B}^{-1}.$

Substitution into the constitutive law results in

$$\mathbb{T} = 2\rho\left\{I_3\left(\frac{\partial\Psi}{\partial I_3}\right)_\theta \mathbb{I}_\mathrm{d} + \left[\left(\frac{\partial\Psi}{\partial I_1}\right)_\theta + I_1\left(\frac{\partial\Psi}{\partial I_2}\right)_\theta\right]\mathbb{B} - \left(\frac{\partial\Psi}{\partial I_2}\right)_\theta \mathbb{B}^2\right\}$$

Volumetric shear strain decomposition

Decomposition of $\mathbb{F}$:
$$\begin{array}{lll} J^{\frac{1}{3}}\mathbb{I}_d & \rightarrow & \text{volumetric part} \\ \overline{\mathbb{F}} = J^{-\frac{1}{3}}\mathbb{F} & \rightarrow & \text{isochoric part} \end{array}$$

The free energy is now expressed as ($\overline{\mathbb{B}} = J^{-\frac{2}{3}}\mathbb{B}$ and $\bar{I}_k \equiv I_k(\overline{\mathbb{B}})$)

$$\Psi \equiv \Psi(J, I_1(\overline{\mathbb{B}}), I_2(\overline{\mathbb{B}}), \theta) = \Psi_v(J, \theta) + \Psi_s(\bar{I}_1, \bar{I}_2, \theta).$$

Ψ_v, Ψ_s are the volumetric and shear parts of the free energy.

Decomposition of the Cauchy stress tensor

$$\mathbb{T} = \underbrace{\rho J \left(\frac{\partial \Psi_v}{\partial J}\right)_\theta}_{=p \text{ volumetric}} \mathbb{I}_d + \underbrace{2\rho \left[\left(\frac{\partial \Psi_s}{\partial \bar{I}_1}\right)_\theta \overline{\mathbb{B}}_0 - \left(\frac{\partial \Psi_s}{\partial \bar{I}_2}\right)_\theta (\overline{\mathbb{B}}^{-1})_0\right]}_{=\mathbb{T}_0 \text{ deviatoric}}$$

Examples of constitutive laws

Pressure and internal energy $\rightarrow$ classical thermodynamical relations

$$p(\tau,\theta) = -\rho^0 \left(\frac{\partial \Psi_v}{\partial J}\right)_\theta, \qquad \varepsilon_v(J,\theta) = \Psi_v(J,\theta) - \theta \left(\frac{\partial \Psi_v}{\partial \theta}\right)_J.$$

Volumetric free energy

$$\Psi_v = \frac{\mu}{4\rho^0}\left((J-1)^2 + (\log J)^2\right) \quad \Rightarrow \quad p = -\frac{\mu}{2}\left(J - 1 + \frac{\log J}{J}\right),$$

use the siffened gas or any but convex EOS to ensure hyperbolicity.

Deviatoric (shear part) free energy: Rank-one convex stored energies

$$\Psi_s(\bar{I}_1,\bar{I}_2) = \frac{\mu}{4\rho^0}\left[-2a(\bar{I}_1 - 3) + \frac{(1+a)}{3}(\bar{I}_2^2 - 9)\right], \qquad a \in [-1; 0.5].$$

$a = -1 \rightarrow$ Neo-Hookean model $\Psi_s = \frac{\mu}{2\rho^0}(\bar{I}_1 - 3)$, Gavrilyuk et al., *J. of Elasticity*, 2015

$a = 0 \rightarrow$ Non-linear law $\Psi_s = \frac{\mu}{12\rho^0}(\bar{I}_2^2 - 1)$

Relation shear modulus as Young modulus and Poisson ration: $\mu = E/(2(1+\nu))$.

Outline

Mesh and geometry - Unstructured simplex

$\omega(t) \rightarrow$ computational domain in dimensions $d \in [2,3]$

$\partial\omega(t) \rightarrow$ boundary of $\omega(t)$ in $d-1$

$\boldsymbol{n} \rightarrow$ outward pointing unit normal vector

c/p index for cell/point

$\mathcal{T}_\omega^n = \bigcup_{c=1}^{N_E} \omega_c^n$ current mesh

$\mathcal{F}(c)/\mathcal{P}(c)$ set of faces/points of c

$\omega_c^{n/n+1}$ current/updated cell

ω_{cp}^n subcell

$\mathcal{C}(p)/\mathcal{F}(p)$ set of cells/faces of point p

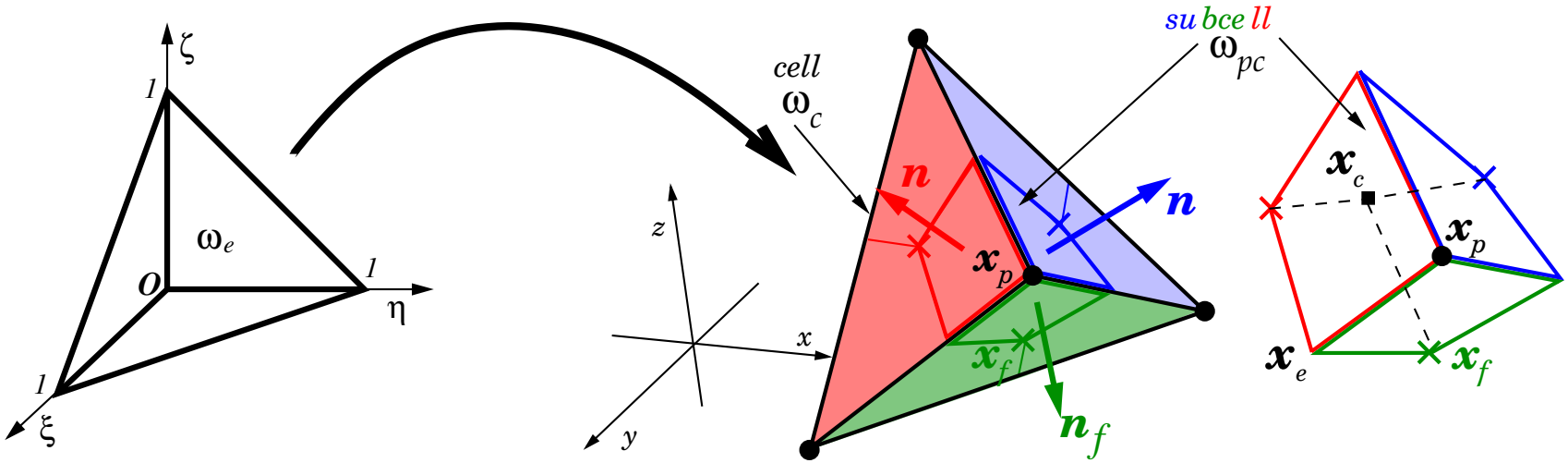

Left: Reference element ω_e in $\boldsymbol{\xi} = (\xi, \eta, \zeta)$ coord. Right: cell ω_c and subcell ω_{pc}.

Discrete velocity gradient operator

Fundamental geometrical object: corner normal vector

$$a_{pc}\boldsymbol{n}_{pc} = \frac{\partial|\omega_c|}{\partial \boldsymbol{x}_p}, \quad \text{such that} \quad \sum_{p\in\mathcal{P}(c)} a_{pc}\boldsymbol{n}_{pc} = \boldsymbol{0}.$$

Interesting geometrical identity: $\displaystyle\sum_{p\in\mathcal{P}(c)} a_{pc}\boldsymbol{x}_p \otimes \boldsymbol{n}_{pc} = |\omega_c|\mathbb{I}_{\mathrm{d}}.$

Discrete velocity gradient/divergence operators

Application of Gauss theorem to $\nabla \boldsymbol{v}$ yields

$$\mathbb{L}_c(\boldsymbol{v}) = \frac{1}{|\omega_c|}\int_{\partial\Omega_c} \boldsymbol{v}\otimes\boldsymbol{n}\,\mathrm{d}s = \frac{1}{|\omega_c|}\sum_{p\in\mathcal{P}(c)} a_{pc}\boldsymbol{v}_p\otimes\boldsymbol{n}_{pc}$$

Taking the trace yields the discrete cell-centered divergence

$$\mathrm{tr}\left[\mathbb{L}_c(\boldsymbol{v})\right] = \frac{1}{|\omega_c|}\sum_{p\in\mathcal{P}(c)} a_{pc}\boldsymbol{v}_p\cdot\boldsymbol{n}_{pc}.$$

Subcell force

The masses of cell/subcell are constant in time:

$$m_{pc} = \int_{\Omega_{pc}} \rho^0(\boldsymbol{X})\,\mathrm{d}V, \quad m_c = \int_{\Omega_c} \rho^0(\boldsymbol{X})\,\mathrm{d}V = \sum_{p\in\mathcal{P}(c)} m_{pc}.$$

Fundamental physical object: The subcell force $\boldsymbol{f}_{pc}$ $\rightarrow$ traction force exerted on the outer boundary of subcell ω_{pc}.

The derivation starts from integration over ω_c of the momentum equation:

$$m_c \frac{\mathrm{d}\boldsymbol{v}_c}{\mathrm{d}t} - \int_{\partial\omega_c} \mathbb{T}\boldsymbol{n}\,\mathrm{d}s = m_c \frac{\mathrm{d}\boldsymbol{v}_c}{\mathrm{d}t} - \sum_{p\in\mathcal{P}(c)} \underbrace{\int_{\partial\omega_{pc}\cap\partial\omega_c} \mathbb{T}\boldsymbol{n}\mathrm{d}s}_{\equiv \boldsymbol{f}_{pc}} = \boldsymbol{0}$$

Semi-discrete scheme for Lagrangian hyperelasticity

Physical PDEs

$$m_c \frac{\mathrm{d}\tau_c}{\mathrm{d}t} - \sum_{p \in \mathcal{P}(c)} a_{pc} \boldsymbol{n}_{pc} \cdot \boldsymbol{v}_p = 0,$$

$$m_c \frac{\mathrm{d}\boldsymbol{v}_c}{\mathrm{d}t} - \sum_{p \in \mathcal{P}(c)} \boldsymbol{f}_{pc} = \boldsymbol{0}$$

$$m_c \frac{\mathrm{d}e_c}{\mathrm{d}t} - \sum_{p \in \mathcal{P}(c)} \boldsymbol{f}_{pc} \cdot \boldsymbol{v}_p = 0$$

"Extra" PDEs

$$\frac{\mathrm{d}\boldsymbol{x}_p}{\mathrm{d}t} = \boldsymbol{v}_p, \quad m_c = \text{constant}$$

$$\frac{\mathrm{d}\mathbb{B}_c}{\mathrm{d}t} - \mathbb{L}_c \mathbb{B}_c - \mathbb{B}_c \mathbb{L}_c^t = 0$$

$$\mathbb{B}_c = \mathbb{F}_c \mathbb{F}_c^t, \; \mathbb{L}_c = (\nabla_x \boldsymbol{v})_c$$

Nodal solver [*Maire*, *JCP*, 2009]: compute nodal velocity $\boldsymbol{v}_p$

$$\sum_{c \in \mathcal{C}(p)} \mathbb{M}_{pc} \boldsymbol{v}_p = \sum_{c \in \mathcal{C}(p)} \mathbb{M}_{pc} \boldsymbol{v}_c - \sum_{c \in \mathcal{C}(p)} a_{pc} \mathbb{T}_c \boldsymbol{n}_{pc}, \quad \mathbb{M}_{pc} = \sum_{f \in \mathcal{F}(pc)} z_f \, A_f \, \boldsymbol{n}_f \otimes \boldsymbol{n}_f.$$

Ensures momentum/energy **conservation** and **thermodynamic** compatibility

Hydrodynamics: $z_f \equiv z_c = \rho_c a_c$. Hyper-elasticity $z_f \equiv z_c = \rho_c \sqrt{a_c^2 + \frac{4}{3} \frac{\mu_c}{\rho_c}}$

Space-time ADER scheme

1. Knowledge of the geometry $\boldsymbol{x}^n$ and variables $\mathbf{Q}_c = (\tau_c, \boldsymbol{v}_c, e_c, \mathbb{B}_c)^n$ at time t^n
2. Nodal solver:

$$\sum_{c \in \mathcal{C}(p)} \mathbb{M}_{pc} \boldsymbol{v}_p^* = \sum_{c \in \mathcal{C}(p)} \mathbb{M}_{pc} \boldsymbol{v}_c^* - a_{pc}^n \mathbb{T}_c^* \boldsymbol{n}_{pc}^n, \quad \mathbb{M}_{pc} = \sum_{f \in \mathcal{F}(pc)} z_f^* A_f^n \boldsymbol{n}_f^n \otimes \boldsymbol{n}_f^n$$

3. Subcell force: $\boldsymbol{f}_{pc}^* = a_{pc}^n \mathbb{T}_c^* \boldsymbol{n}_{pc}^n + \mathbb{M}_{pc}(\boldsymbol{v}_p^* - \boldsymbol{v}_c^*)$
4. Update geometry: $\boldsymbol{x}_p^{n+1} = \boldsymbol{x}_p^n + \Delta t \, \boldsymbol{v}_p^*$
5. Update physical variables:

$$\tau_c^{n+1} = \tau_c^n + \frac{\Delta t}{m_c} \sum_{p \in \mathcal{P}(c)} \widetilde{a_{pc} \boldsymbol{n}_{pc}} \cdot \boldsymbol{v}_p^*, \qquad \widetilde{a_{pc} \boldsymbol{n}_{pc}} = \frac{1}{\Delta t} \int_{t^n}^{t^{n+1}} a_{pc} \, \boldsymbol{n}_{pc} \, \mathrm{d}t$$

$$\boldsymbol{v}_c^{n+1} = \boldsymbol{v}_c^n + \frac{\Delta t}{m_c} \sum_{p \in \mathcal{P}(c)} \boldsymbol{f}_{pc}^*, \qquad e_c^{n+1} = e_c^n + \frac{\Delta t}{m_c} \sum_{p \in \mathcal{P}(c)} \boldsymbol{f}_{pc}^* \cdot \boldsymbol{v}_p^*$$

Space-time ADER scheme

Space-time 2nd order representations (predictors)

Solution/geometry representation with space-time nodal functions $\theta_l(\boldsymbol{\xi}, \tau)$:

$$\mathbf{q}_h = \sum_{l=1}^{\mathcal{L}} \theta_l(\boldsymbol{\xi}, \tau) \widehat{\mathbf{q}}_{l,c}, \qquad \boldsymbol{x}_h = \sum_{l=1}^{\mathcal{L}} \theta_l(\boldsymbol{\xi}, \tau) \widehat{\boldsymbol{x}}_{l,c}, \qquad \mathcal{L} = 2\mathcal{M}, \quad \mathcal{M} = d + 1,$$

with $\mathbf{q}_h = (\tau, \boldsymbol{v}, e, \mathbb{B})_h$.

Space: Unlimited constrained central reconstruction [Dumbser et al, JCP, 2007]

$$\frac{1}{|\omega_j^n|} \int_{\omega_j^n} \sum_{l=1}^{\mathcal{M}} \theta_l(\boldsymbol{\xi}, 0)\, \widehat{\mathbf{q}}_{l,c}\, \mathrm{d}v \simeq \mathbf{Q}_j^n, \quad \mathcal{S}_c = \bigcup_{j=1}^{n_e} \omega_{m(j)}^n, \qquad \forall \omega_j^n \in \mathcal{S}_c$$

$$\frac{1}{|\omega_c^n|} \int_{\omega_c^n} \sum_{l=1}^{\mathcal{M}} \theta_l(\boldsymbol{\xi}, 0)\, \widehat{\mathbf{q}}_{l,c}\, \mathrm{d}v = \mathbf{Q}_c^n. \qquad \leftarrow \text{constrains}$$

Space-time ADER scheme

Time: ADER scheme [Titarev and Toro, *J. Sci. Comput.*, 2002]

Weak form of the PDEs

$$\int_{t^n}^{t^{n+1}} \int_{\omega_c(t)} \theta_k(\boldsymbol{\xi},\tau) \left(\frac{\mathrm{d}\mathbf{q}_h}{\mathrm{d}t} - \frac{1}{\rho_h} \nabla \cdot \mathbf{f}(\mathbf{q}_h, \nabla \mathbf{q}_h) \right) \mathrm{d}v \, \mathrm{d}t = 0,$$

$$\int_{t^n}^{t^{n+1}} \int_{\omega_c(t)} \theta_k(\boldsymbol{\xi},\tau) \frac{\mathrm{d}\boldsymbol{x}}{\mathrm{d}t} \, \mathrm{d}v \, \mathrm{d}t = \int_{t^n}^{t^{n+1}} \int_{\omega_c(t)} \theta_k(\boldsymbol{\xi},\tau) \, \boldsymbol{v} \, \mathrm{d}v \, \mathrm{d}t,$$

with $\mathbf{q}_h = (\tau, \boldsymbol{v}, e, \mathbb{B})_h$ and $\mathbf{f}(\mathbf{q}_h, \nabla \mathbf{q}_h) = (\boldsymbol{v}, \mathbb{T}, \mathbb{T}\boldsymbol{v}, \mathbb{L}\mathbb{B} - \mathbb{B}\mathbb{L}^t)_h$.

The values at time t^* in the nodal solver are fed using $\mathbf{q}^*(\boldsymbol{x}) = \mathbf{q}_h(\boldsymbol{x}, t^*)$ for any space-time coordinate $(\boldsymbol{x}, t^*)$.

Space-time discretization of the geometry equation for $\mathbb{B}$

Time differentiation of $\mathbb{F}_c$

in the Eulerian reference frame

$$\frac{\mathrm{d}\mathbb{F}_c}{\mathrm{d}t} - \frac{1}{|\omega_c|}\sum_{p\in\mathcal{P}(c)} a_{pc}(\boldsymbol{v}_p \otimes \boldsymbol{n}_{pc})\mathbb{F}_c = 0 \qquad \Rightarrow \qquad \frac{\mathrm{d}\mathbb{F}_c}{\mathrm{d}t} - \mathbb{L}_c\mathbb{F}_c = 0.$$

Crank-Nicolson scheme in $[t^n, t^{n+1}]$

$$\mathbb{F}_c^{n+1} - \mathbb{F}_c^n - \frac{\Delta t}{2}\mathbb{L}_c^{n+\frac{1}{2}}(\mathbb{F}_c^{n+1} + \mathbb{F}_c^n) = 0, \qquad \mathbb{L}_c^{n+\frac{1}{2}} = \frac{1}{|\omega_c^{n+\frac{1}{2}}|}\sum_{p\in\mathcal{P}(c)} a_{pc}^{n+\frac{1}{2}}\boldsymbol{v}_p^{n+\frac{1}{2}} \otimes \boldsymbol{n}_{pc}^{n+\frac{1}{2}}$$

$\mathbb{L}_c^{n+\frac{1}{2}}$ the time-centered approximation of the discrete velocity gradient. Then

$$\mathbb{F}_c^{n+1} = \left(\mathbb{A}_c^-\right)^{-1}\left(\mathbb{A}_c^+\right)\mathbb{F}_c^n, \qquad \mathbb{A}_c^{\pm} = \mathbb{I}_\mathrm{d} \pm \frac{\Delta t}{2}\mathbb{L}_c^{n+\frac{1}{2}}, \quad \Delta t > 0 \text{ s.t. } \det(\mathbb{A}_c) > 0.$$

2nd order update of $\mathbb{B}_c$ consistent with discrete Jacobian

$$\mathbb{B}_c^{n+1} = \left(\mathbb{A}_c^-\right)^{-1}\left(\mathbb{A}_c^+\right)\mathbb{B}_c^n\left(\mathbb{A}_c^+\right)^\top\left(\mathbb{A}_c^-\right)^{-\top}$$

preserves symmetry and ≥ 0 definiteness of the left Cauchy-Green tensor.

A posteriori MOOD limiter [Clain et al., *JCP*, 2011]

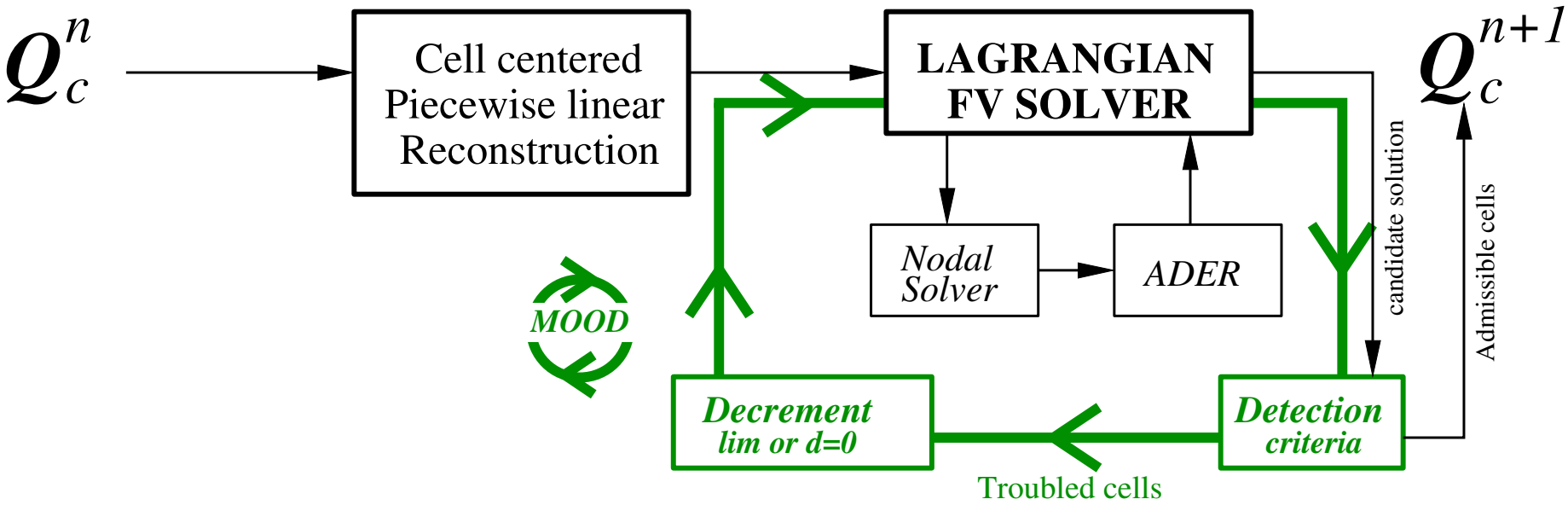

Sketch of the current Lagrangian numerical method and the associated MOOD loop with decrementing: $\mathbb{P}_1 \rightarrow \mathbb{P}_1^{\text{LIM}} \rightarrow \mathbb{P}_0$

A posteriori MOOD limiter [Clain et al., *JCP*, 2011]

1. $\mathbb{P}_1$: *Accuracy* is gained with the unlimited piecewise-linear polynomial reconstruction: maximal second-order of accuracy, possibly oscillating;
2. $\mathbb{P}_1^{\text{lim}}$: *Robustness* is gained with the previous reconstruction supplemented with Barth-Jespersen (BJ) slope limiter: between first- and second-order of accuracy, essentially-non-oscillatory;
3. $\mathbb{P}_0$: *Fail-safe* is gained without any polynomial reconstruction: first-order of accuracy, robust but dissipative.

Numerical admissibility Relaxed Discrete Maximal Principle $\delta_0 = 10^{-4}$, $\delta_1 = 10^{-3}$

$$-\delta_c^n + m_c^n \leq \rho_c^{*,n+1} \leq M_c^n + \delta_c^n, \quad \text{with} \quad \begin{cases} \delta_c^n = \max(\delta_0, \delta_1 |M_c^n - m_c^n|), \\ m_c^n = \min_{d \in \mathcal{V}_c}(\rho_d^n), \quad M_c^n = \max_{d \in \mathcal{V}_c}(\rho_d^n) \end{cases}$$

Physical admissibility: $\tau_c > 0$, $\varepsilon_c > 0$, $\theta_c > 0$. Can add $|\omega_{cp}| > 0$.

Computer admissibility: no `NaN`, `Inf`

Time step restrictions

Computation of the time step

$$\Delta t = \min\left(\Delta t_{\text{volume}},\ \Delta t_{\text{acoustic}},\ \Delta t_{\text{increase}}\right)$$

$$\Delta t_{\text{volume}} = C_v \min_c \left(\frac{|\omega_c^n|}{\sum_{p \in \mathcal{P}(c)} a_{pc} \boldsymbol{n}_{pc} \cdot \boldsymbol{v}_p} \right), \qquad C_v = 0.2$$

$$\Delta t_{\text{acoustic}} = C_{\text{CFL}} \min_c \left(\frac{L_c}{z_c/\rho_c} \right), \qquad z_c/\rho_c = \sqrt{a_c^2 + \frac{4}{3}\frac{\mu_c}{\rho_c}}$$

$$\Delta t_{\text{increase}} = C_i(t^n - t^{n-1}), \qquad C_i = 0.1 \qquad C_{\text{CFL}} = 0.25$$

Outline

Numerical convergence studies – Kidder problem

Isentropic compression of a shell (perfect gas) with exact solution 2D/3D

2D	**Pressure**						**Radius**			
$h(\Omega(t_{\text{final}}))$	ϵ_{L_1}	$\mathcal{O}(L_1)$	ϵ_{L_2}	$\mathcal{O}(L_2)$	ϵ_{L_∞}	$\mathcal{O}(L_\infty)$	$\epsilon_{R_{int}}$	$\mathcal{O}(R_{int})$	$\epsilon_{R_{ext}}$	$\mathcal{O}(R_{ext})$
2.40E-02	2.71E+00	-	6.06E+00	-	2.24E+01	-	2.01E-02	-	5.84E-02	-
1.37E-02	9.34E-01	1.9	2.56E+00	1.5	1.61E+01	0.6	1.57E-02	0.4	5.55E-02	0.1
4.51E-03	5.72E-02	2.5	2.10E-01	2.2	2.79E+00	1.6	2.50E-03	1.7	8.77E-03	1.7

3D	**Pressure**						**Radius**			
$h(\Omega(t_{\text{final}}))$	ϵ_{L_1}	$\mathcal{O}(L_1)$	ϵ_{L_2}	$\mathcal{O}(L_2)$	ϵ_{L_∞}	$\mathcal{O}(L_\infty)$	$\epsilon_{R_{int}}$	$\mathcal{O}(R_{int})$	$\epsilon_{R_{ext}}$	$\mathcal{O}(R_{ext})$
2.18E-02	3.57E+00	-	7.47E+00	-	5.55E+01	-	3.93E-02	-	1.35E-01	-
1.66E-02	2.34E+00	1.6	5.08E+00	1.4	4.68E+01	0.6	2.65E-02	1.5	1.31E-01	0.1
1.20E-02	1.11E+00	2.3	2.76E+00	1.9	3.77E+01	0.7	1.19E-02	2.4	6.74E-02	2.0

Table: Numerical errors and convergence rates with second order of accuracy Lagrange ADER scheme. The error norms refer to the variable p (pressure) or to the internal and external radial position at the final time $t = t_{\text{final}}$.

Numerical convergence studies – Kidder problem

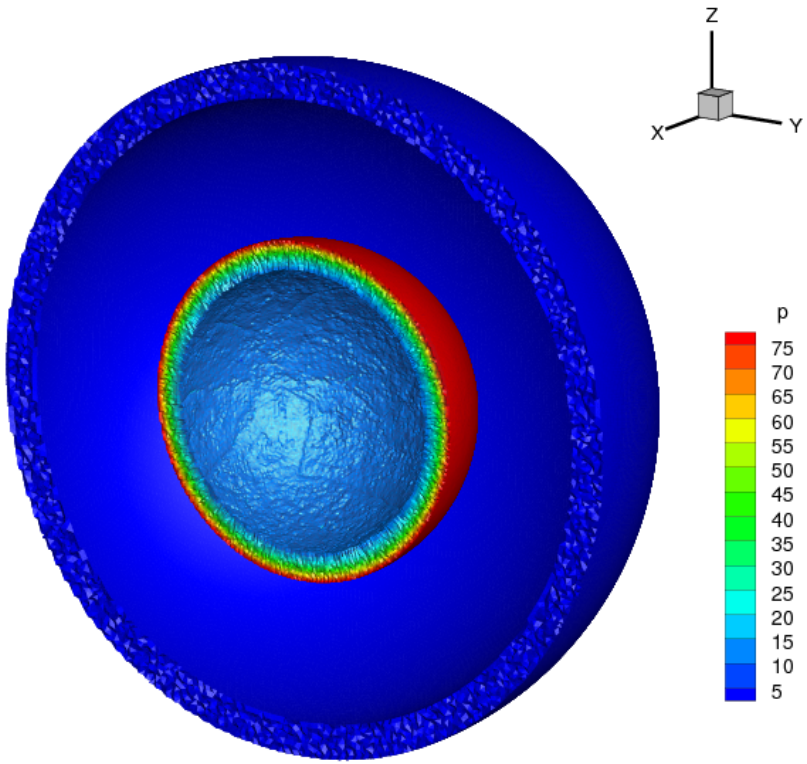

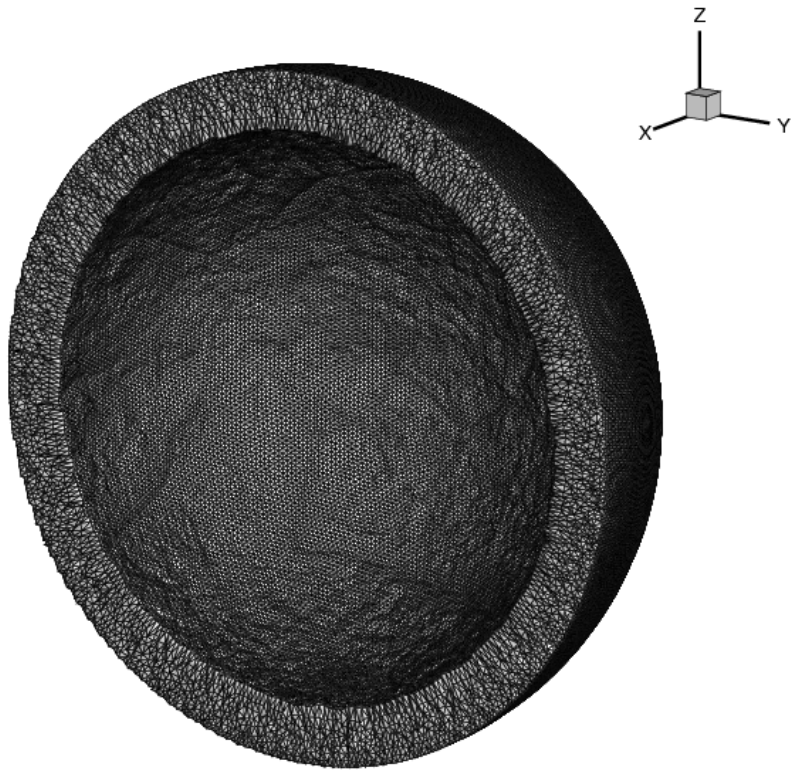

Numerical results – Sod explosion problem

Sod ICs in cylindrical (2D, 70k cells) or spherical (3D, 2.5M cells) geometry

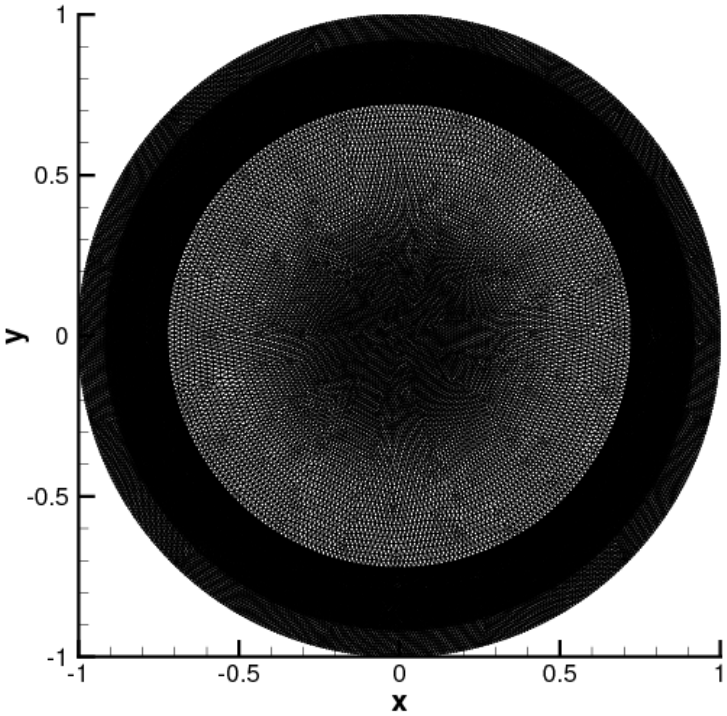

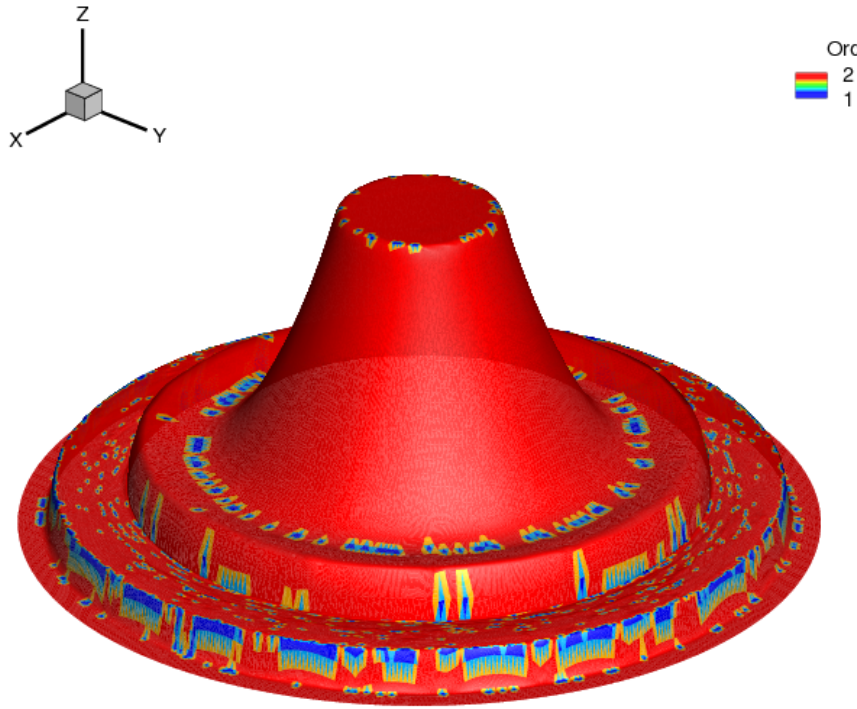

Numerical results – Sod explosion problem

Density (left), pressure (right) for 1st order (blue) and 2nd order (black)

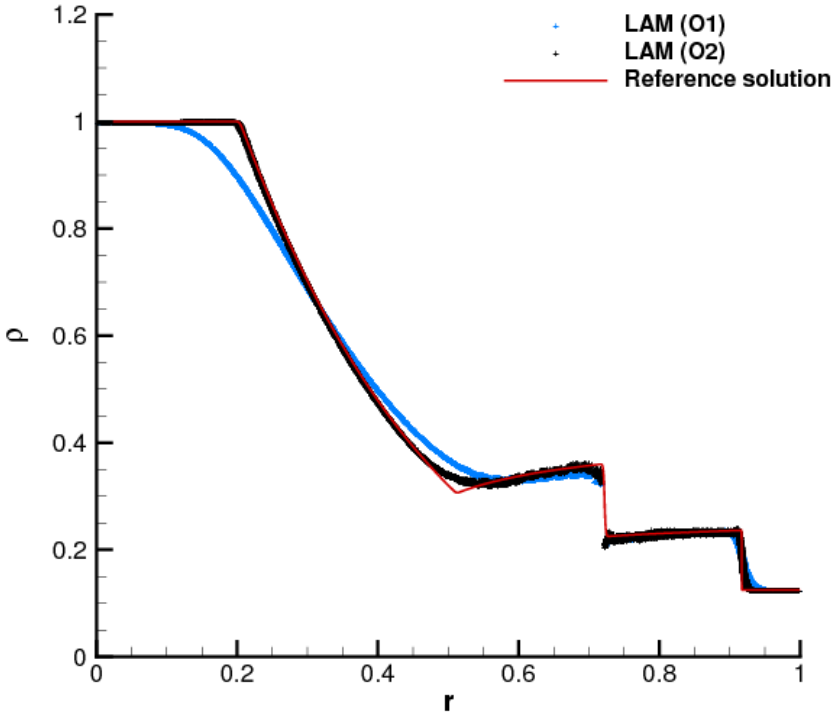

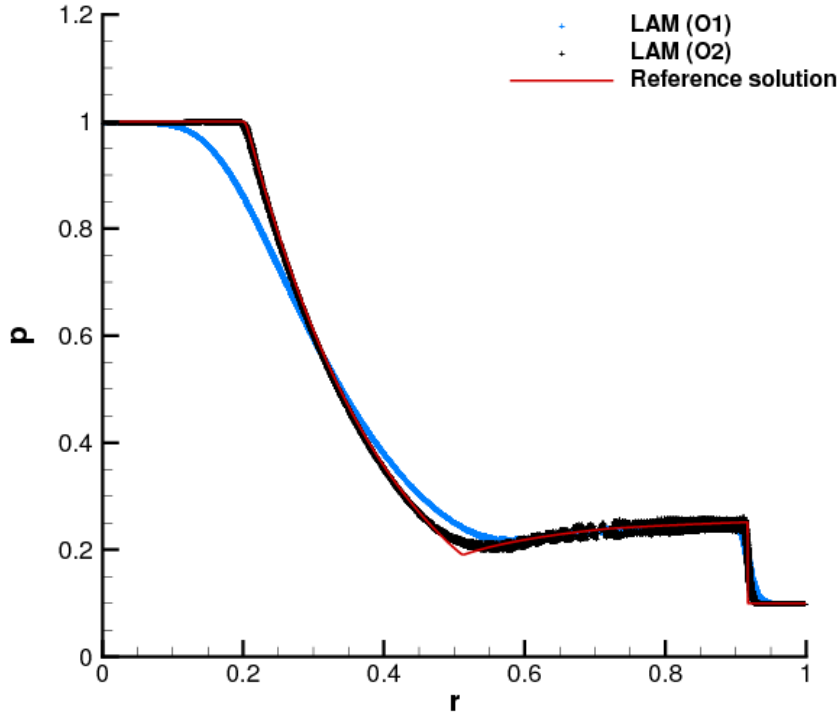

Numerical results – Sod explosion problem

Percent of bad recomputed cells (left: 2D, right:3D)

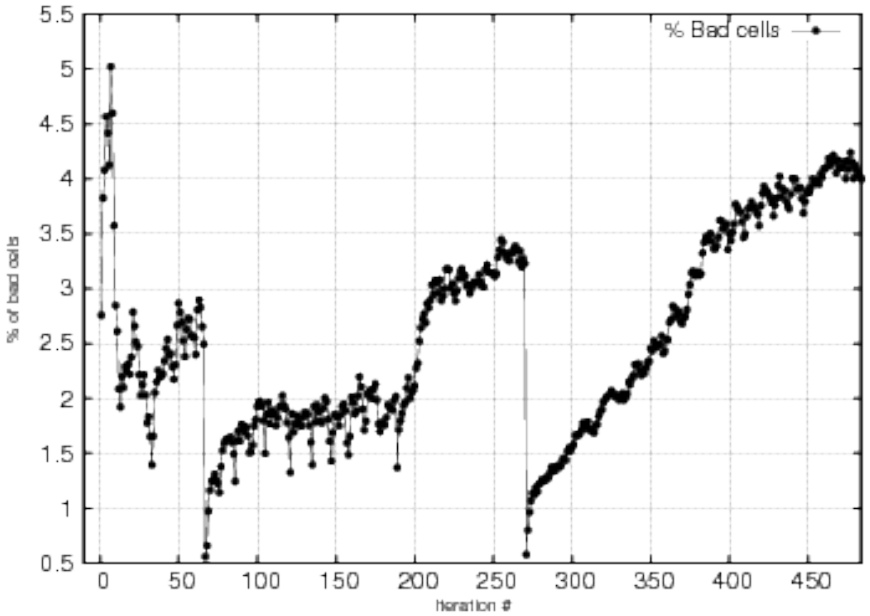

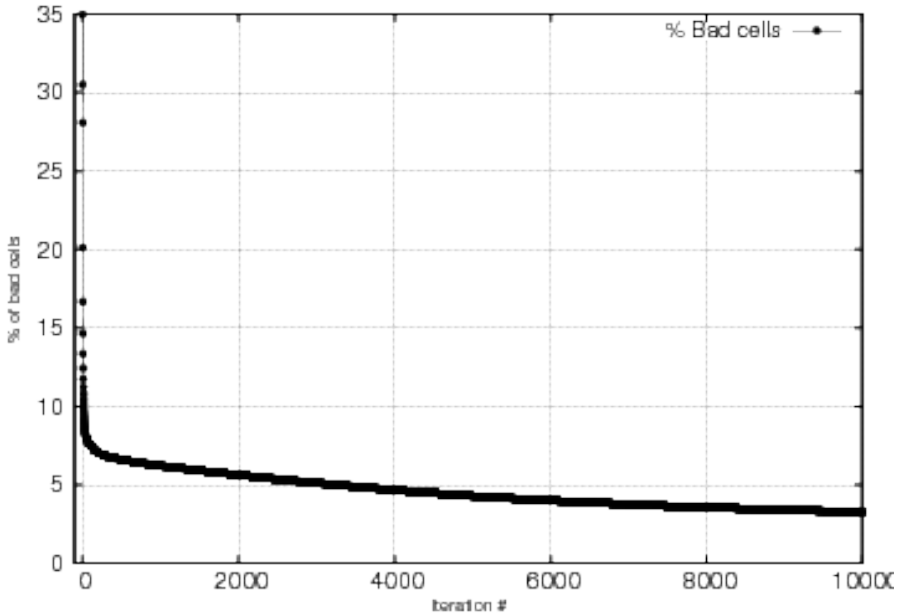

Numerical results – Piston problem

Piston moving from left to right. Initial meshes 9k (2D), 75k (3D) cells

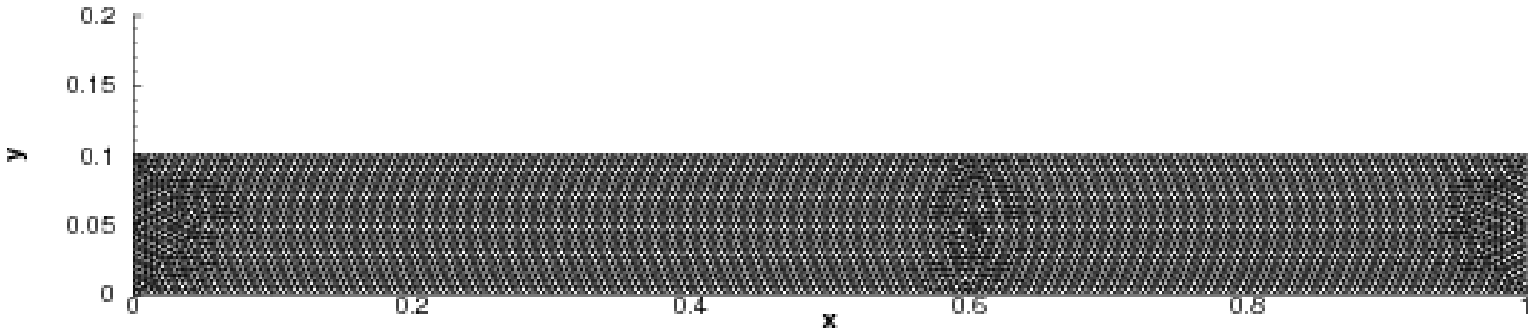

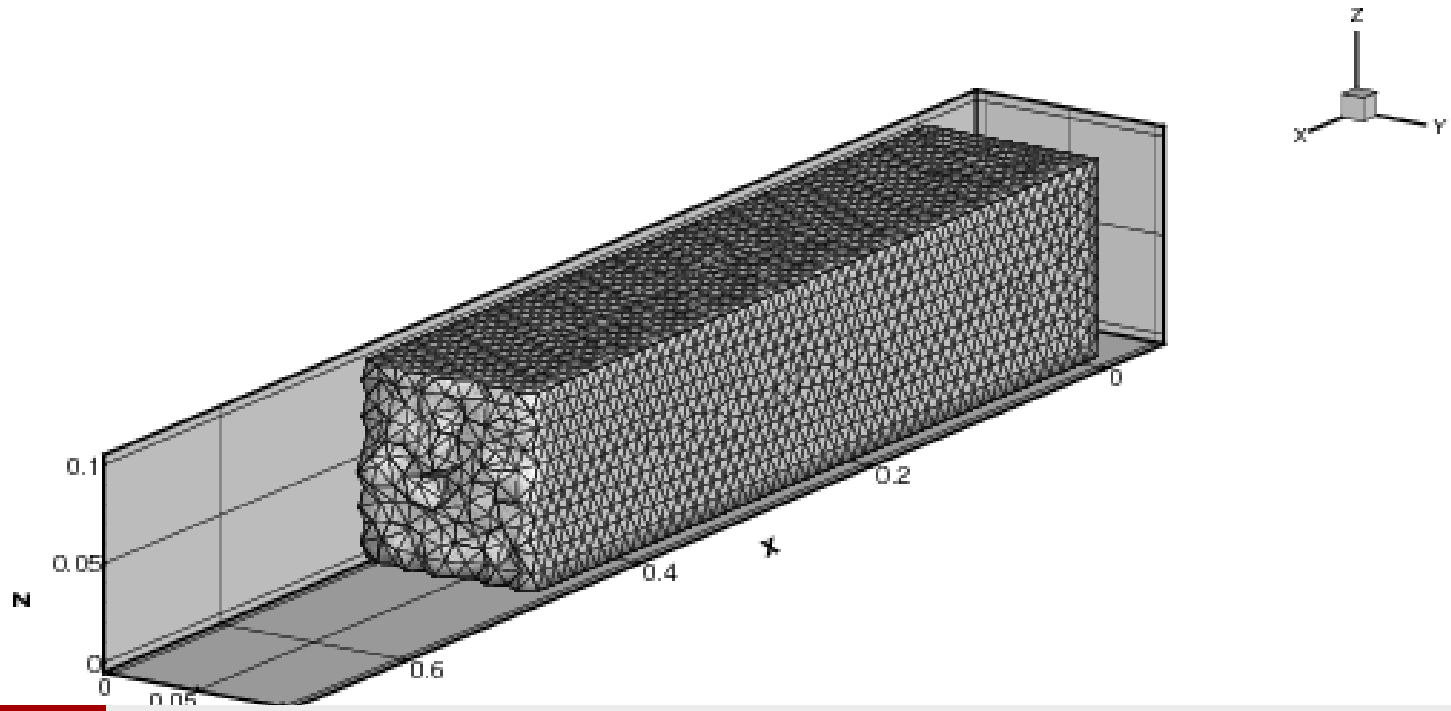

Numerical results – Piston problem

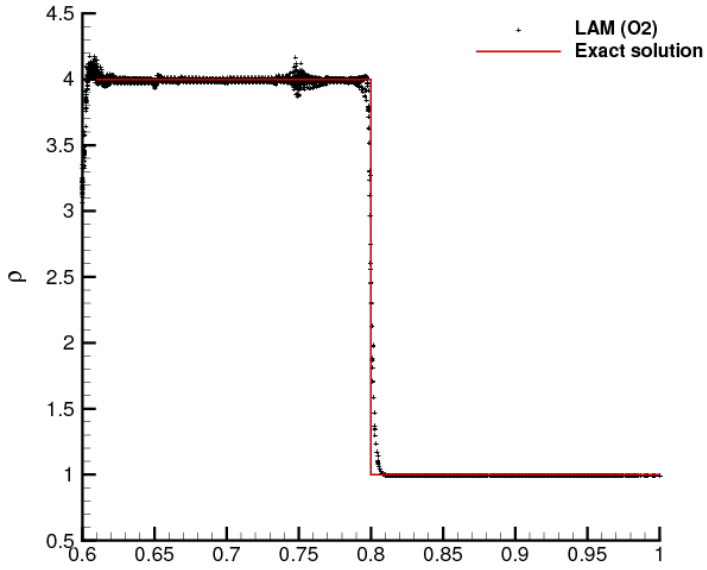

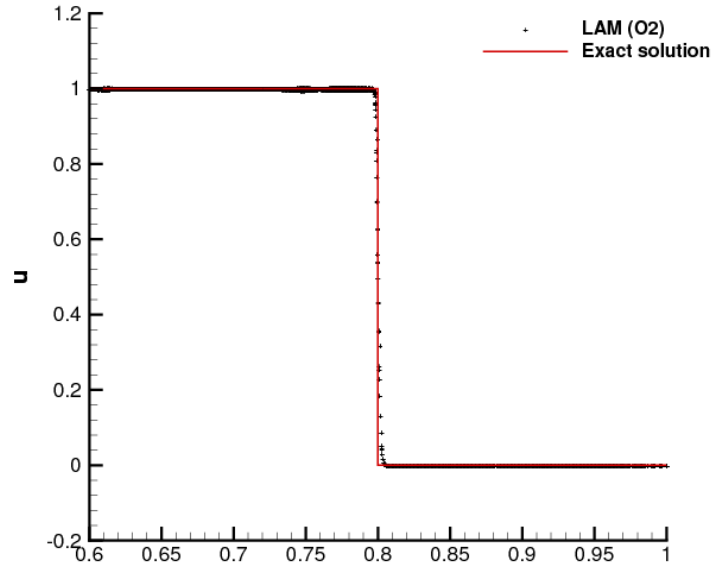

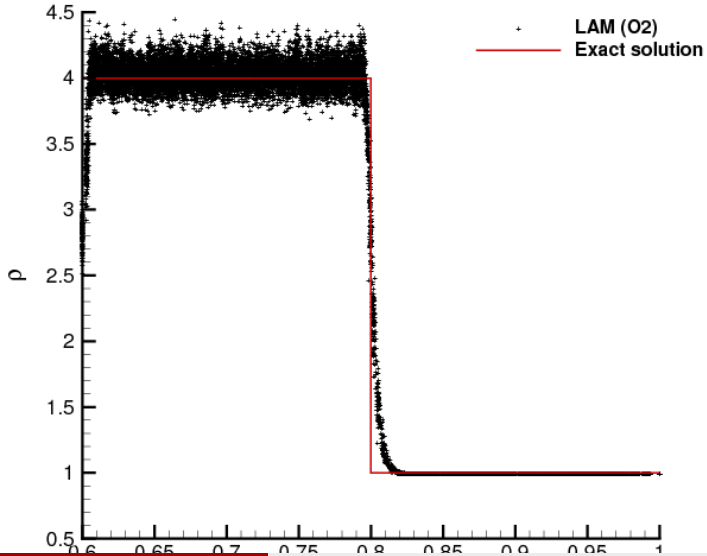

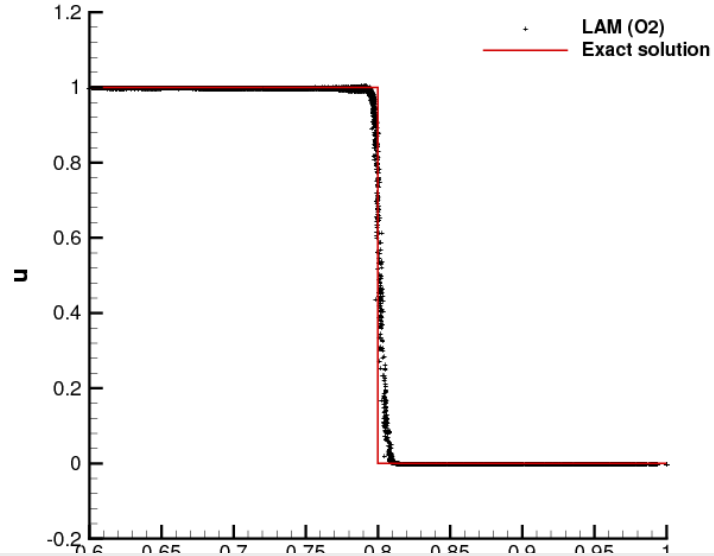

Numerical results – Piston problem

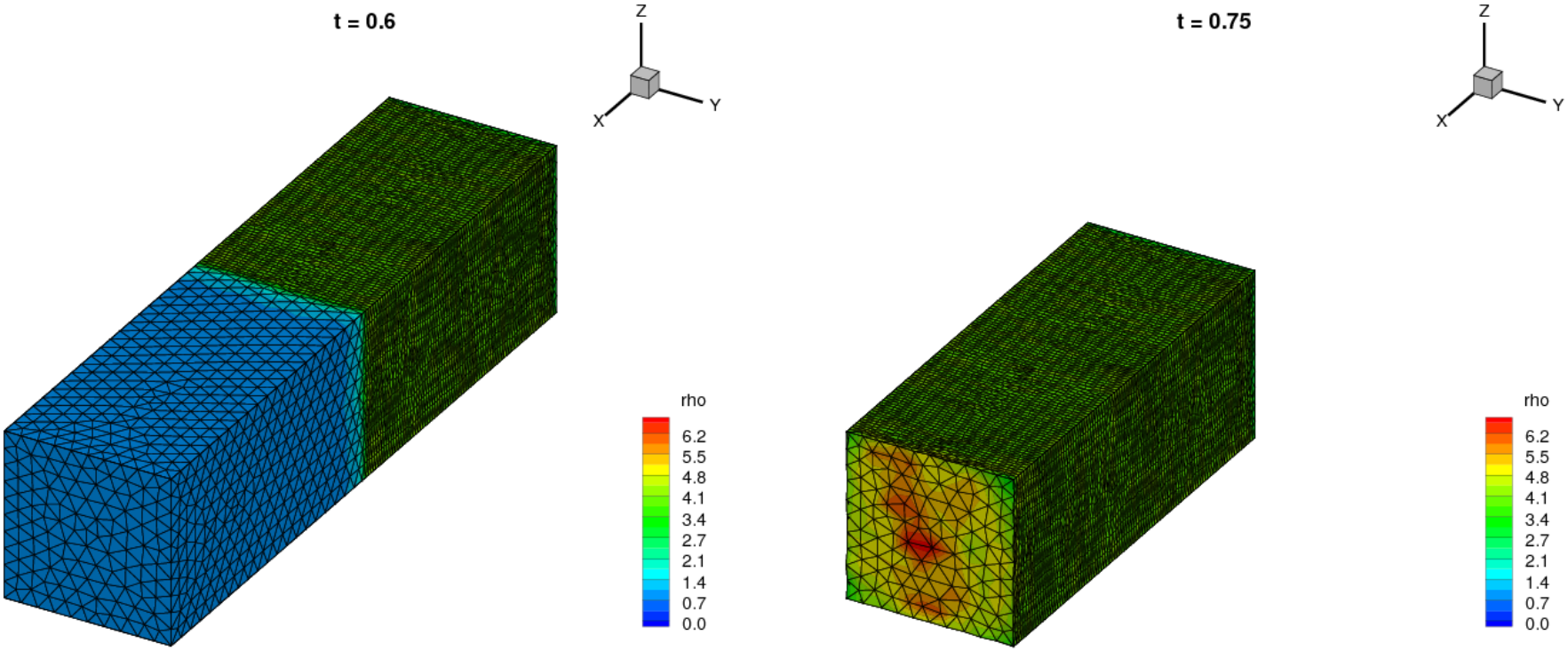

Multiple rebounds of the shock wave on the right wall and moving piston.

Numerical results – Piston problem

Percent of bad cells in 2D (left) and 3D (right)

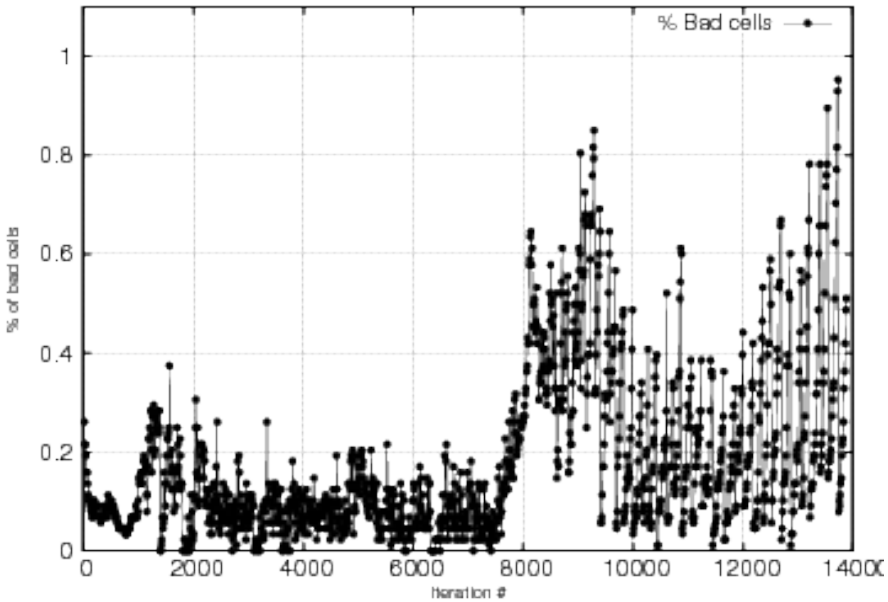

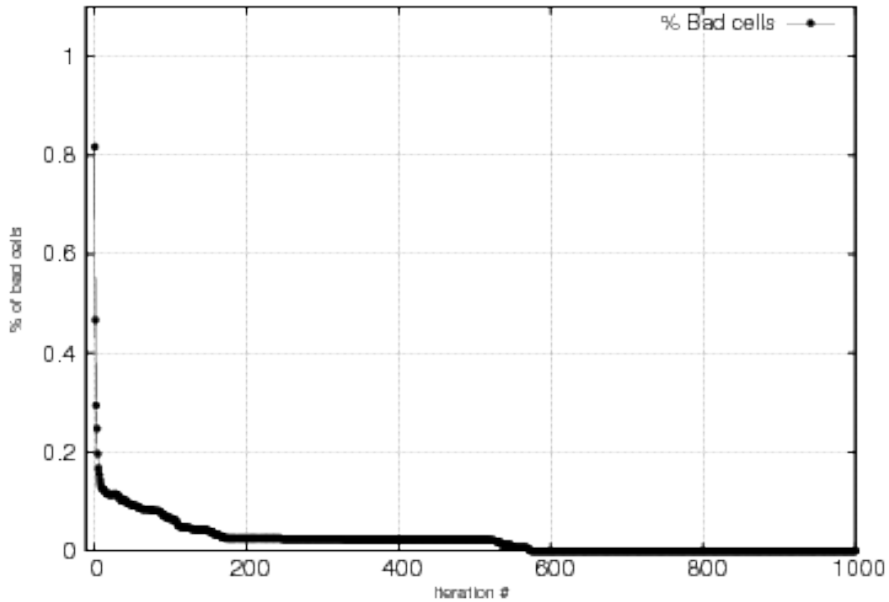

Very few cells are recomputed $\Longrightarrow$ no cost due to MOOD loop!

More tests in hydro: Sedov explosion (2D/3D), linear phase of Richtmyer-Meshkov instability, comparisons and validations. Skipped today.

Outline

Numerical convergence studies

2D Swinging plate test [Scovazzi et al., *IJNME*, 2016]. Domain $\Omega = [0,2]^2$ the smooth solution for the velocity is

$$\boldsymbol{v}^{ex} = \omega U_0 \cos(\omega t) \begin{pmatrix} -\sin\left(\frac{\pi}{2}x\right)\cos\left(\frac{\pi}{2}y\right) \\ \cos\left(\frac{\pi}{2}x\right)\sin\left(\frac{\pi}{2}y\right) \end{pmatrix}, \omega = \frac{\pi}{2}\sqrt{\frac{2\mu}{\rho^0}}, \; U_0 = 5 \cdot 10^{-4} \text{ m}$$

Material: $\rho^0 = 1100$ kg.m^{-3}, Young's $E = 1.7 \cdot 10^7$ Pa, Poisson $\nu = 0.45$.

$L_c(\omega(t_{\text{final}}))$	$\epsilon(u)$	$\mathcal{O}(u)$	$\epsilon(\mathbb{B}_{11})$	$\mathcal{O}(\mathbb{B}_{11})$	$\epsilon(\mathbb{T}_{11})$	$\mathcal{O}(\mathbb{T}_{11})$
7.81E-02	2.144E-03	—	1.581E-04	—	9.681E+02	—
5.21E-02	8.206E-04	2.37	7.072E-05	1.98	4.258E+02	2.03
3.91E-02	4.650E-04	1.97	3.914E-05	2.06	2.343E+02	2.08
3.13E-02	3.085E-04	1.84	2.473E-05	2.06	1.477E+02	2.07
2.60E-02	2.212E-04	1.82	1.699E-05	2.06	1.015E+02	2.06
Expected orders $\rightarrow$		2		2		2

L_2 Numerical errors and convergence rates with second order Lagrange ADER scheme at time $t_{\text{final}} = \pi/\omega$. Variables u (horizontal velocity), $\mathbb{B}_{11}$ and $\mathbb{T}_{11}$.

Elastic vibration of a Beryllium plate

Initial velocity distribution:

$$v^0(x) = A\omega \left[a_1(\sinh(x') + \sin(x')) - a_2(\cosh(x') + \cos(x')) \right], \quad x' = \alpha(x+L/$$

Domain:	$L = 0.06$ m
Parameters:	$\alpha = 78.834$ m^{-1}, $A = 4.3369 \times 10^{-5}$ m
	$\omega = 2.3597 \times 10^5$ s^{-1}, $a_1 = 56.6368$ and $a_2 = 57.6455$
Final time :	$t_{\text{final}} = 3 \cdot 10^{-5}$ s
Material	$\rho^0 = 1845$ kg.m^{-3}, $E = 3.1827 \cdot 10^{11}$ Pa and $\nu = 0.0539$.

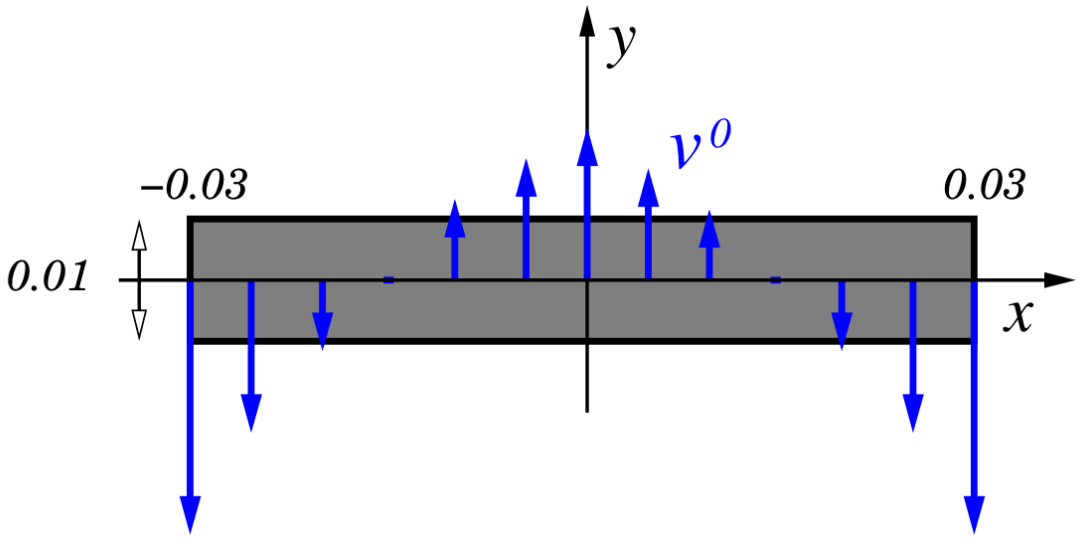

Elastic vibration of a Beryllium plate

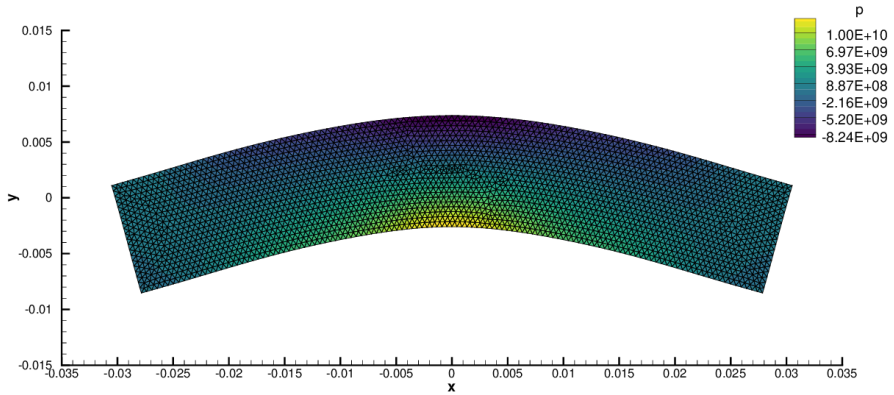

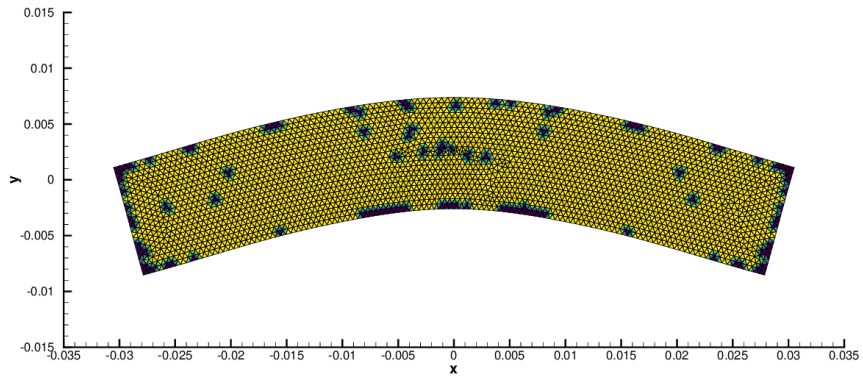

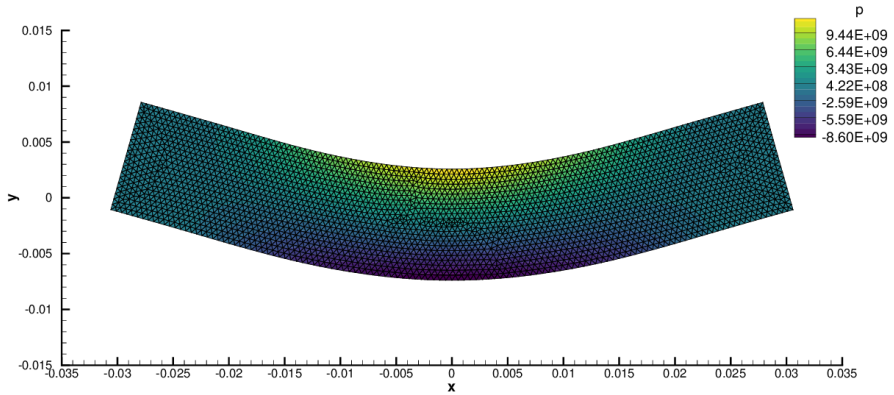

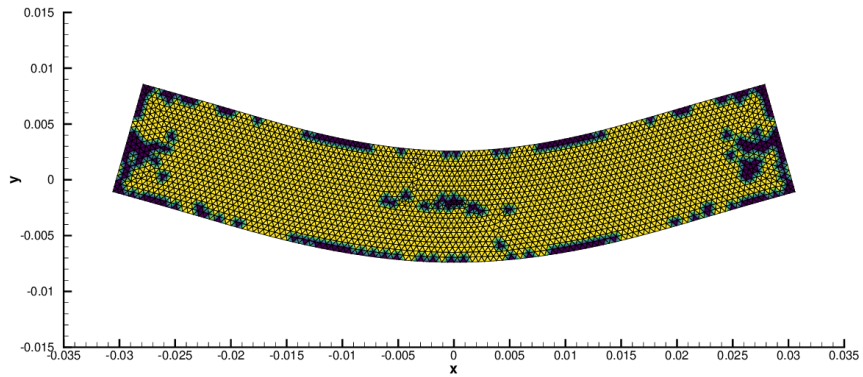

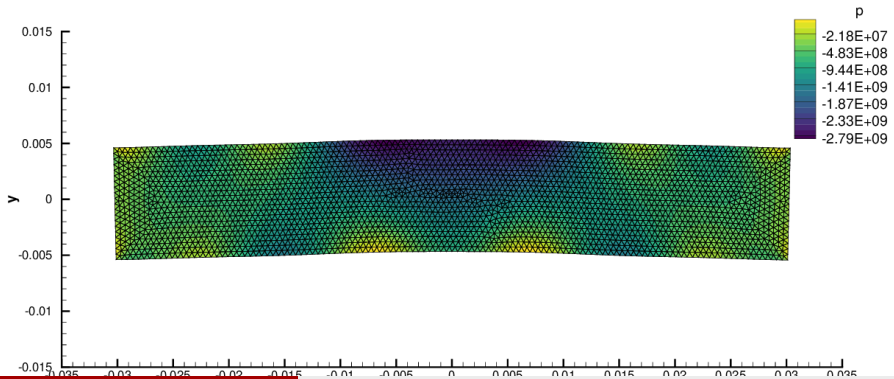

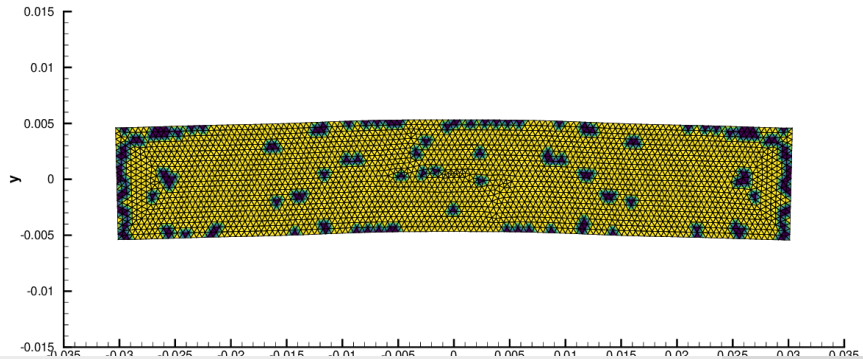

Elastic vibration of a Beryllium plate

Comparison $\mathbb{P}_1 \rightarrow \mathbb{P}_1^{\text{lim}} \rightarrow \mathbb{P}_0$ vs $\mathbb{P}_1 \rightarrow \mathbb{P}_0$

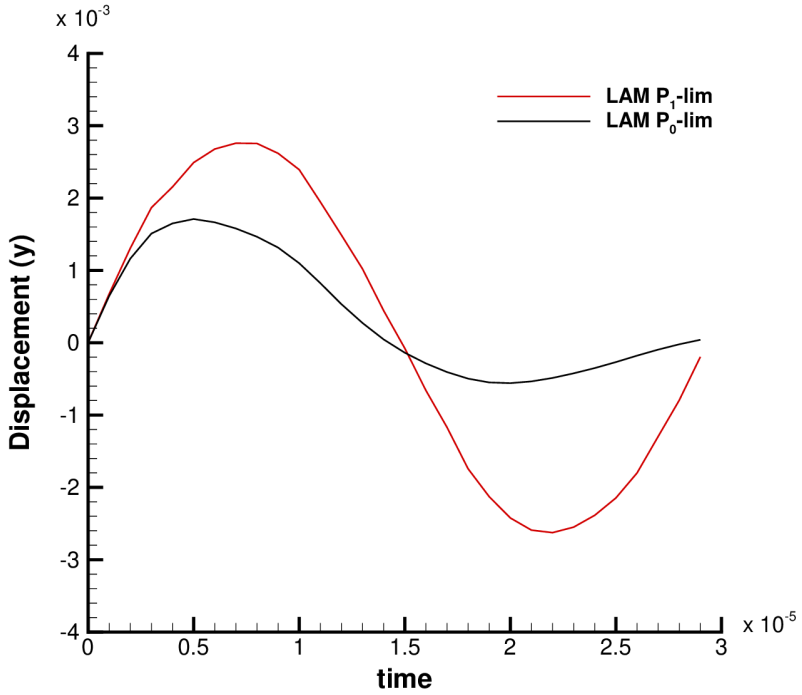

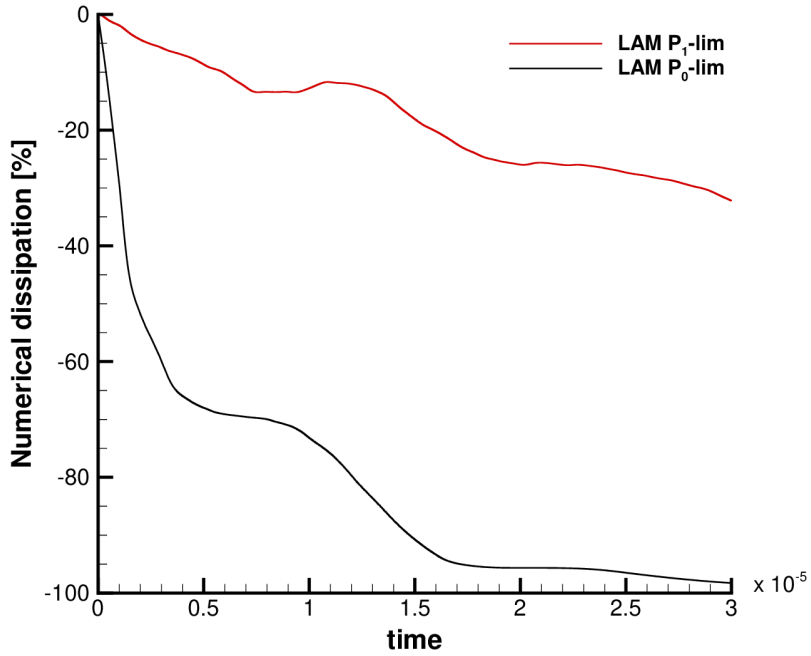

Numerical dissipation measure

$$\delta = \frac{\Psi + k - E_0}{E_0} \qquad \text{with} \quad k_0 =, \qquad E_0 = \Psi_0 + k_0.$$

Blake's problem

Analytical solution is derived from small strain linear elasticity theory [Kamm et al., *TR-LANL*, 2009]

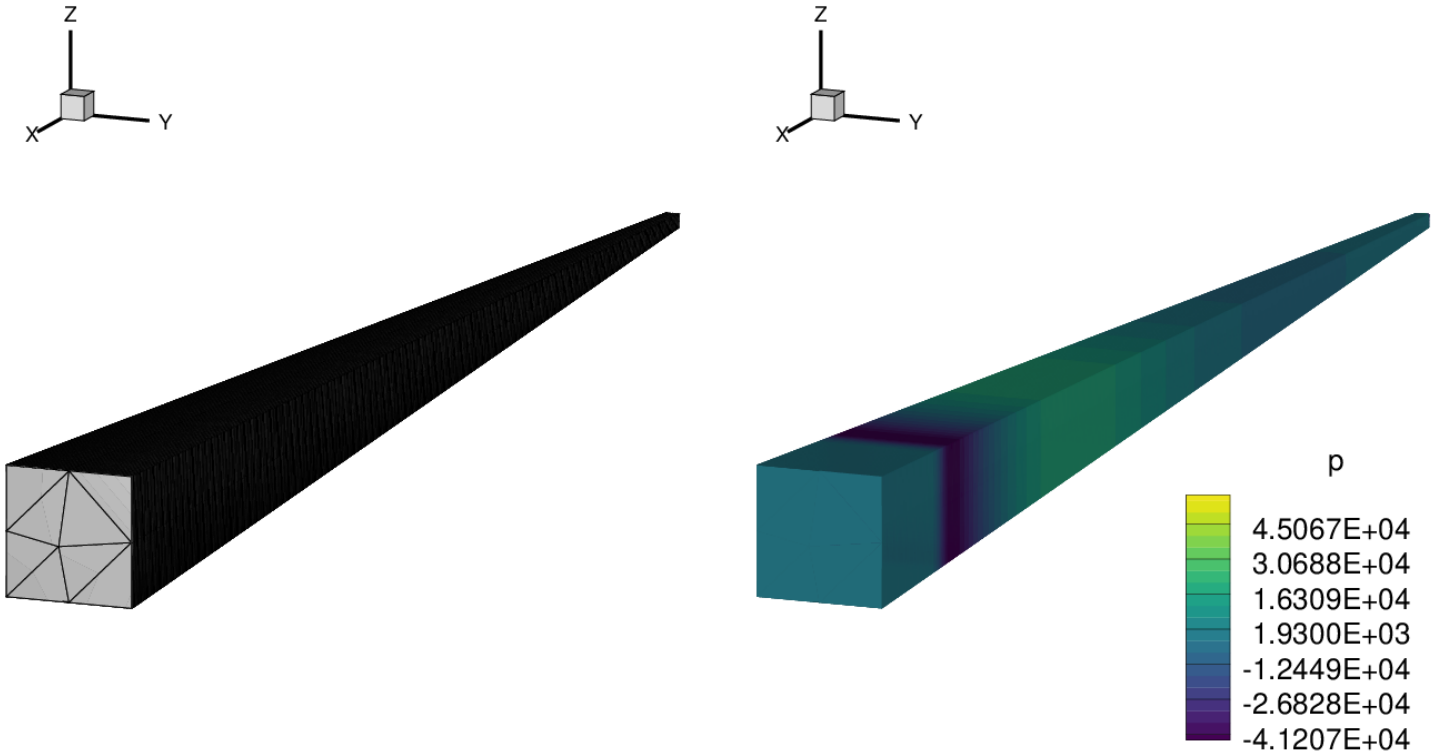

Computational needle: $\omega = [r, \theta, \phi] = [0.9, \pi/180, \pi/180]$

Computational mesh: $h = 1/N_s$ with $N_s = 1000s$ cells $(s = 1, 2, 3)$

Material: $\rho_0 = 3000$ kg.m^{-3}, $E = 62.5 \cdot 10^9$ Pa, $\nu = 0.25$.

Blake's problem

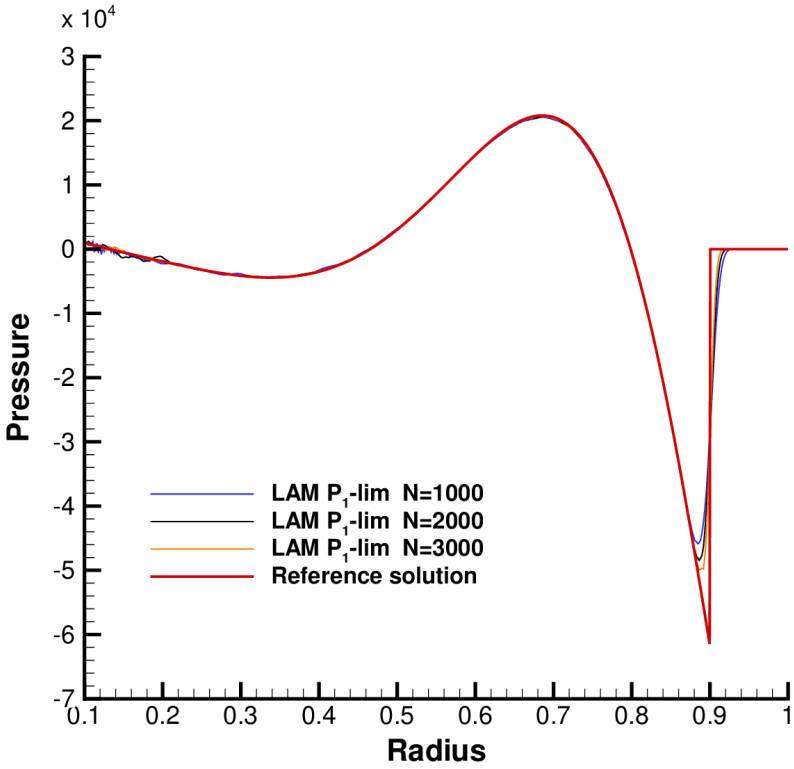

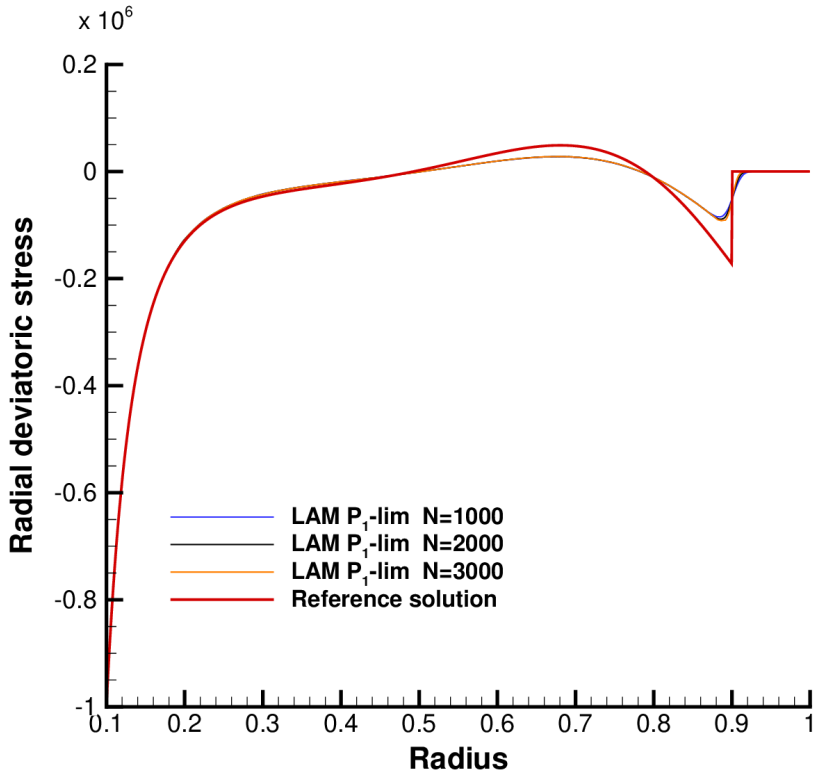

Left: pressure. Right: Radial deviatoric stress

Blake's problem

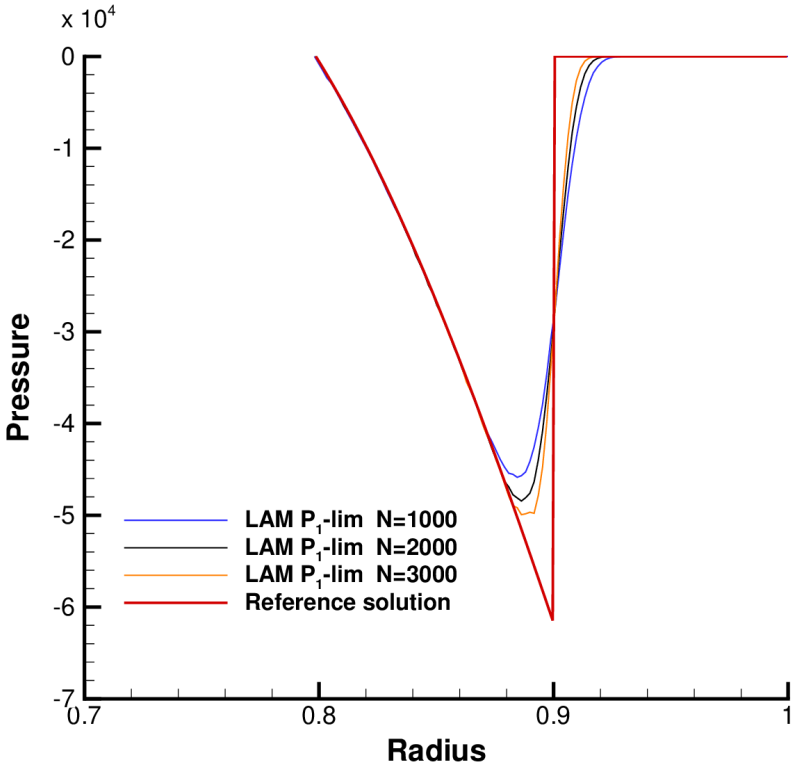

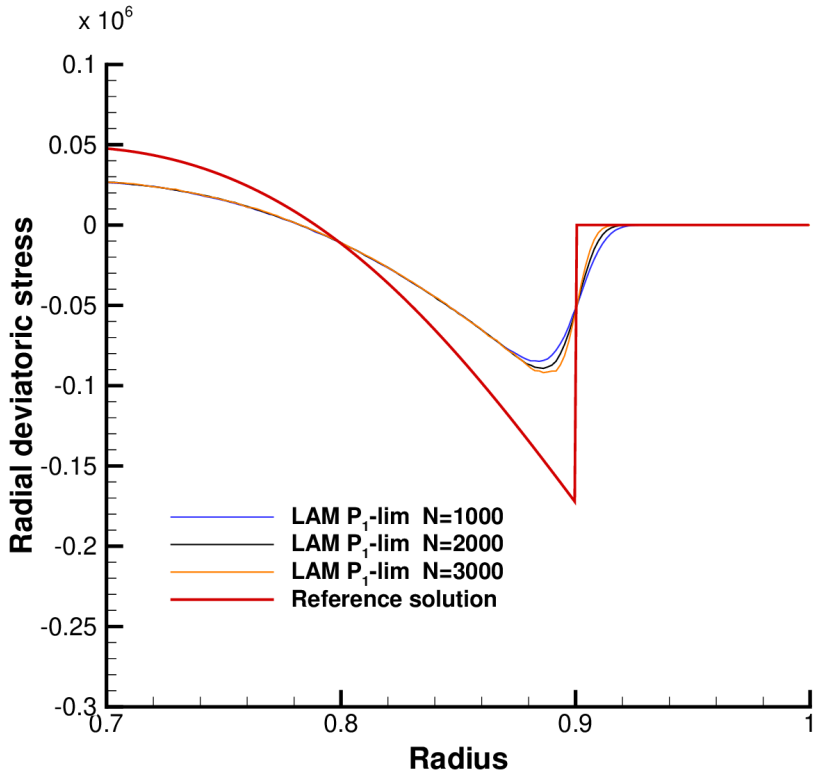

Left: pressure. Right: Radial deviatoric stress

Nearly incompressible solid simulations in 3D

Three configurations: twisting column (Left), rebound of a hollow circular bar (middle) and L-shaped problem (right). Poisson ratio $\nu = 0.45$.

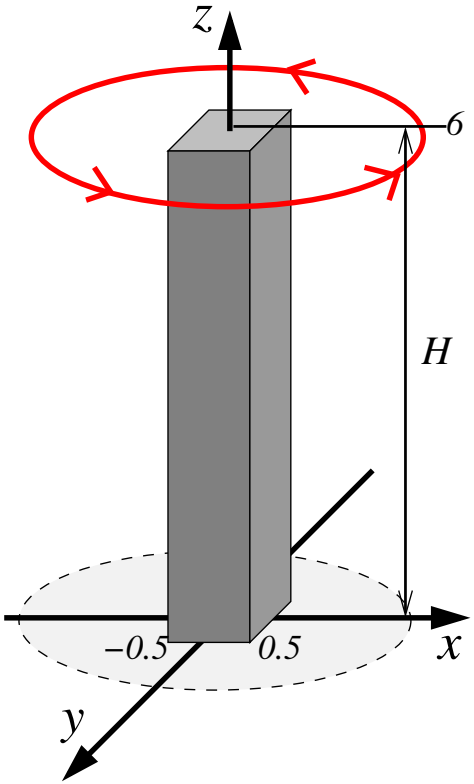

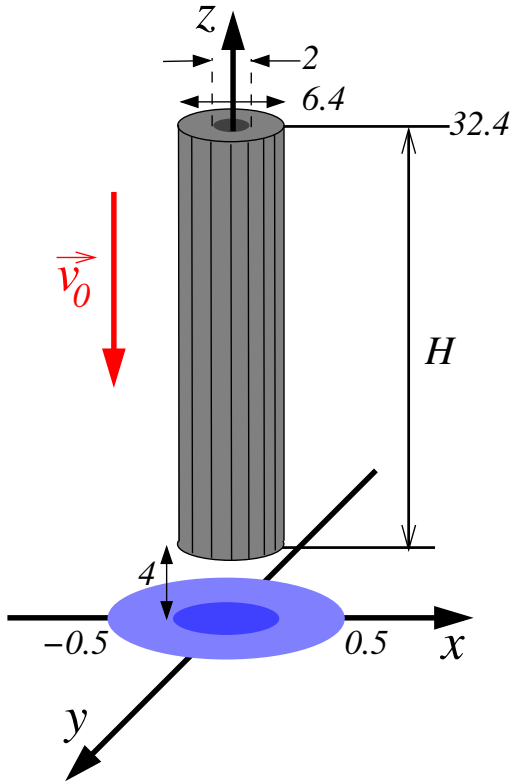

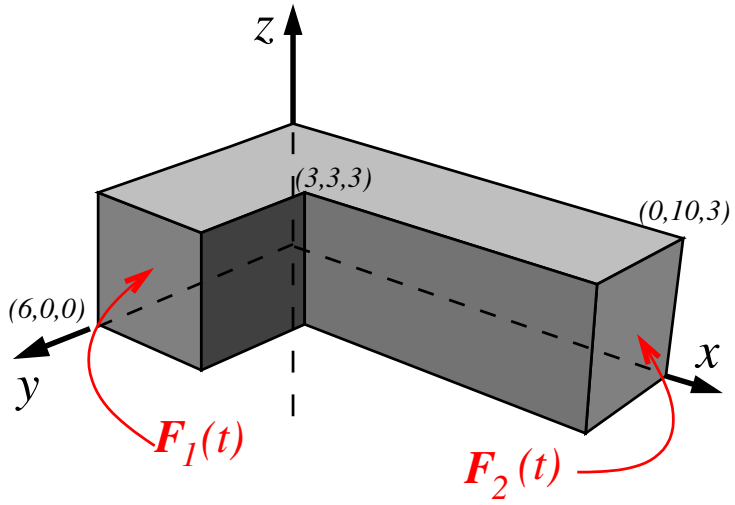

Twisting column

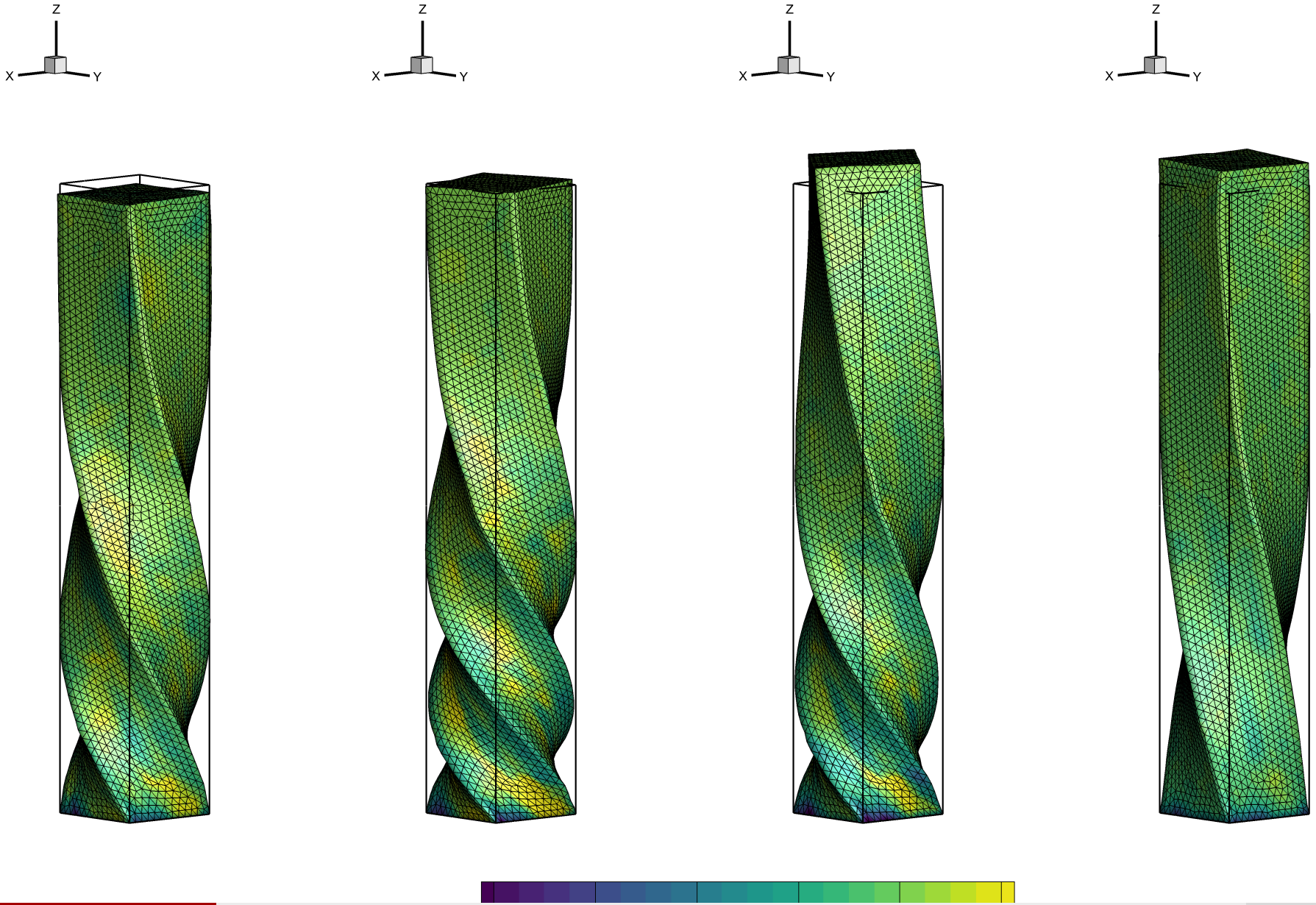

Twisting column

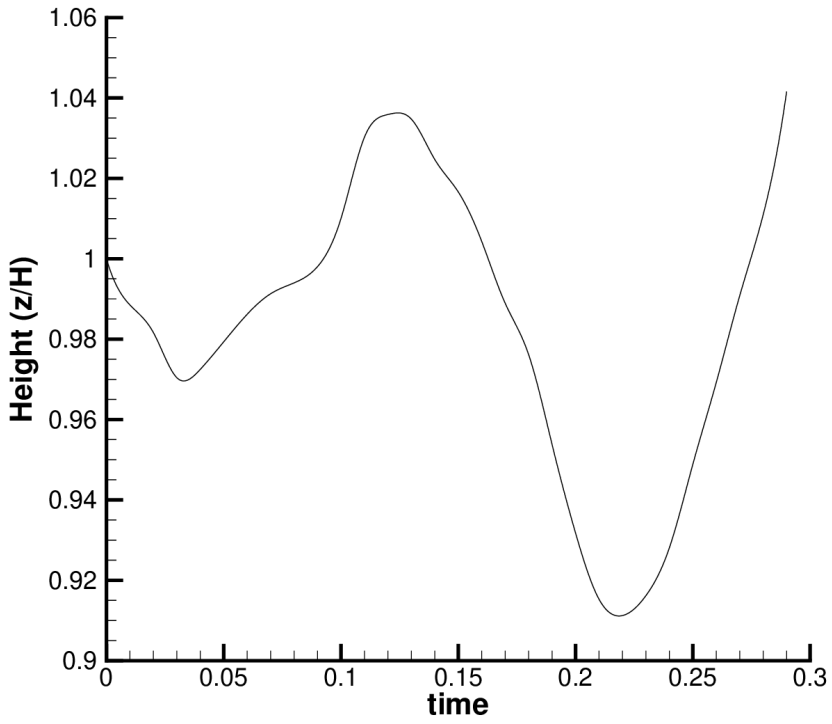

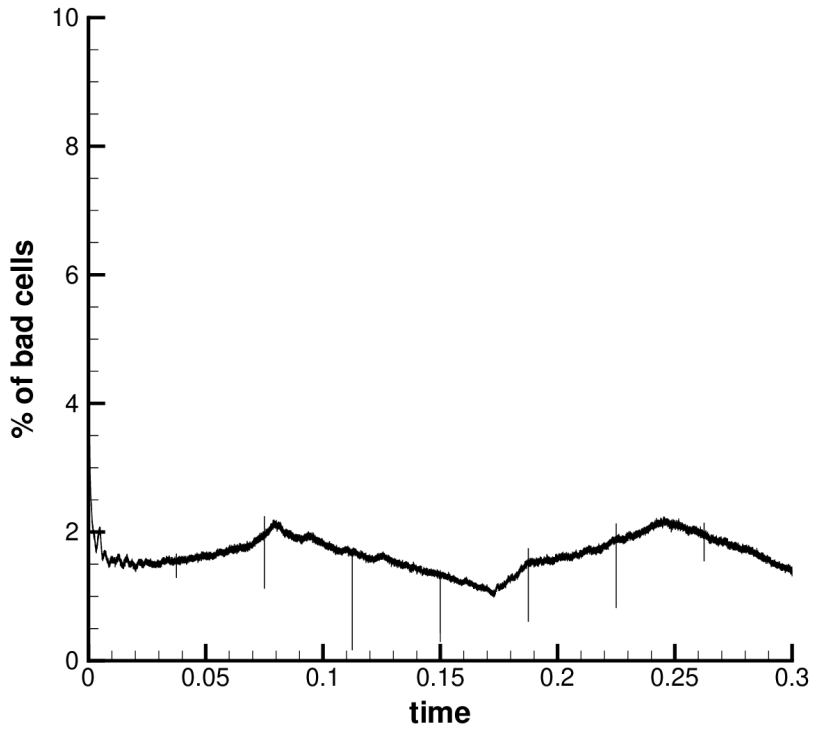

Twisting column — Time evolution of non-dimensional height of the column measured at initial point $\mathbf{x}_T = (0, 0, 6)$ (left). Percentage of bad cells detected (right).

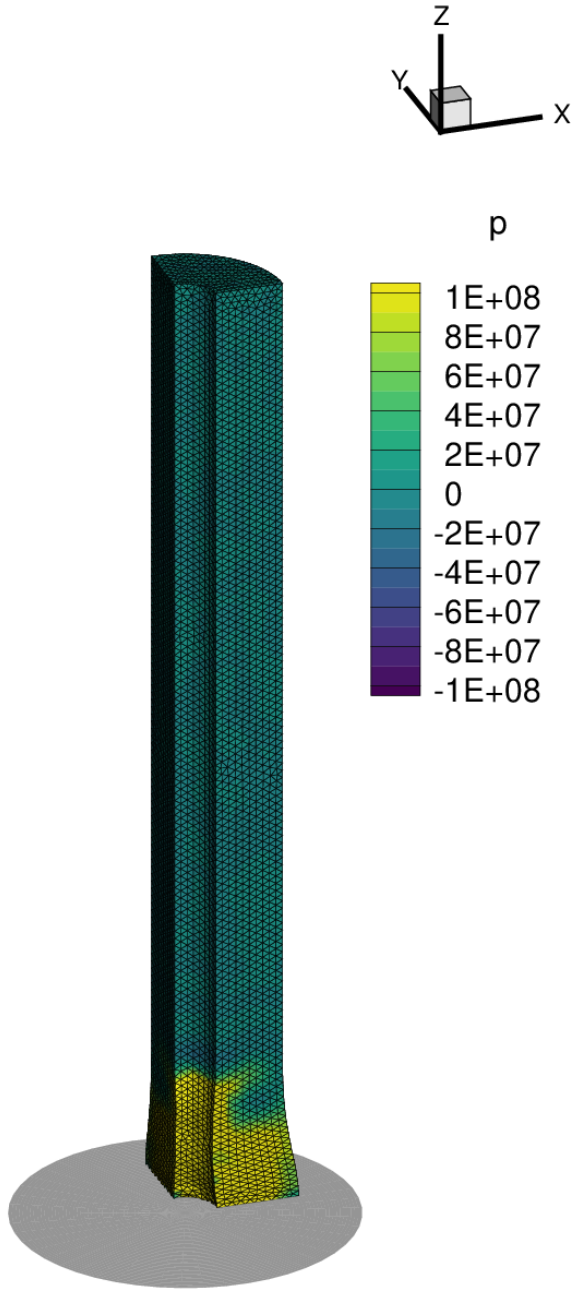
Z
Y
X
p
1E+08
8E+07
6E+07
4E+07
2E+07
0
-2E+07
-4E+07
-6E+07
-8E+07
-1E+08

Rebound of a hollow bar

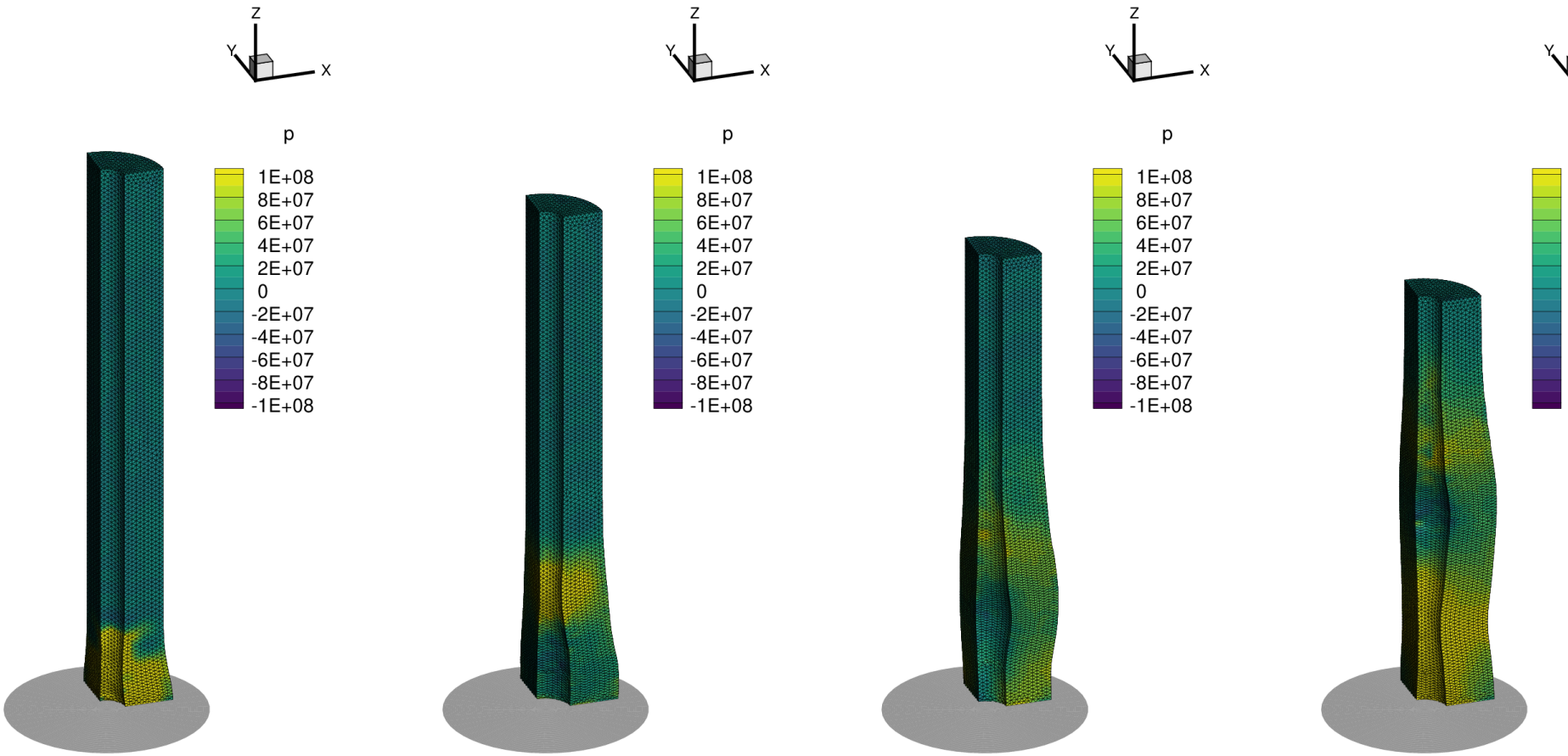

Rebound of a hollow bar

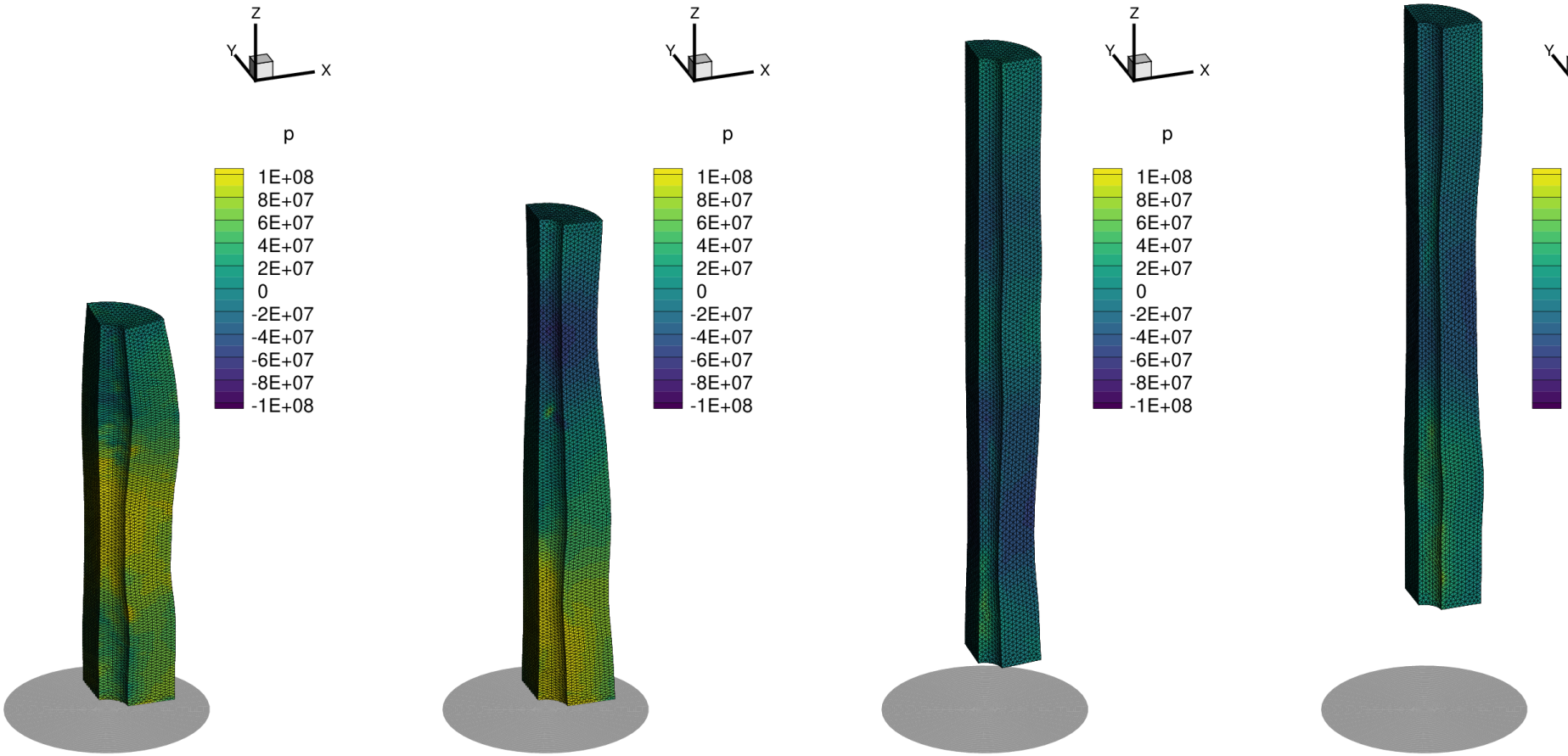

Rebound of a hollow bar

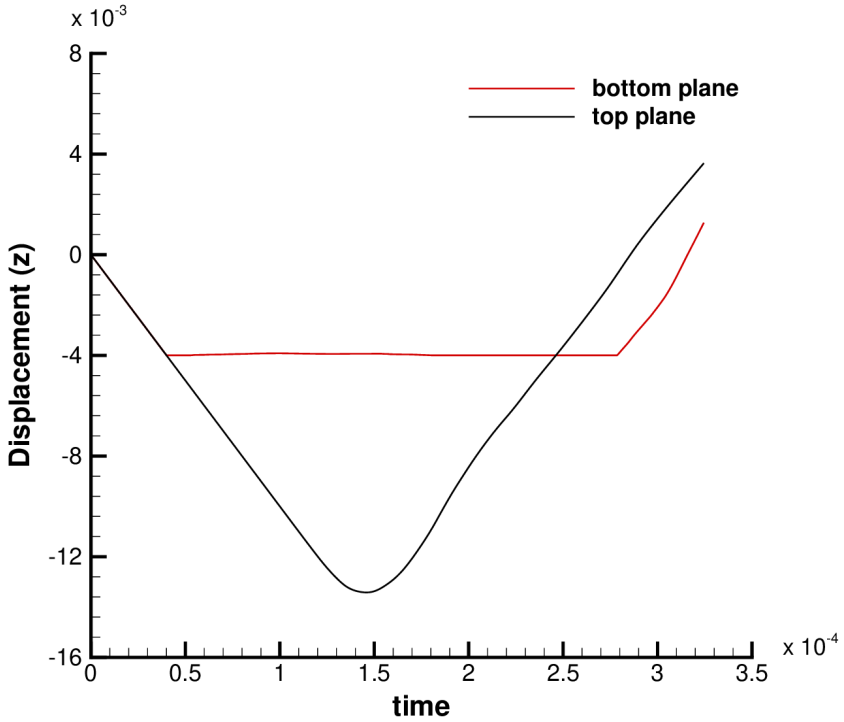

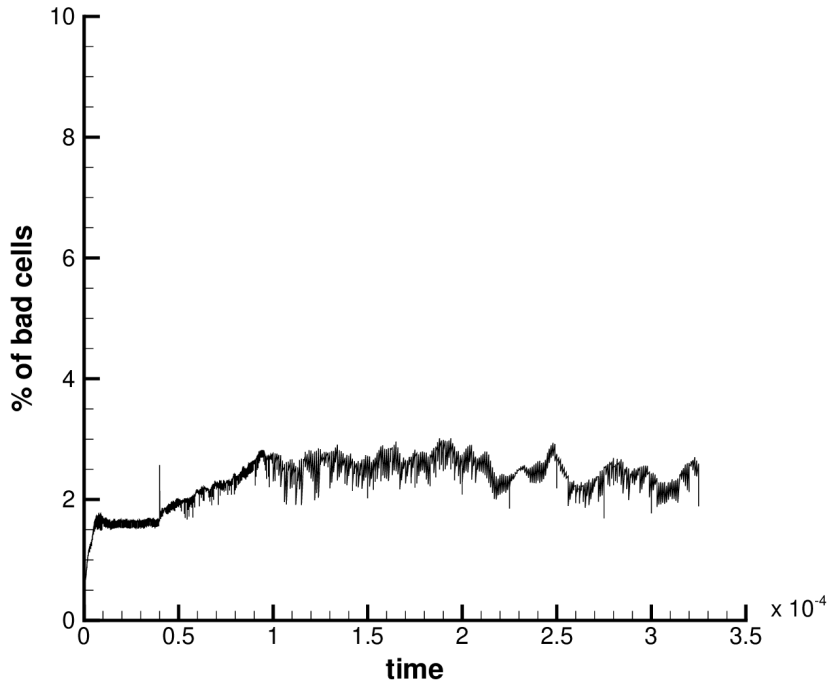

Time evolution of vertical displacement of the points on the top plane $\mathbf{x}_T = (1.6, 0, 32.4) \cdot 10^{-3}$m and on the bottom plane $\mathbf{x}_B = (1.6, 0, 4) \cdot 10^{-3}$m (left) and percentage of bad cells detected at each time step (right).

L-shaped problem – Angular momentum conservation

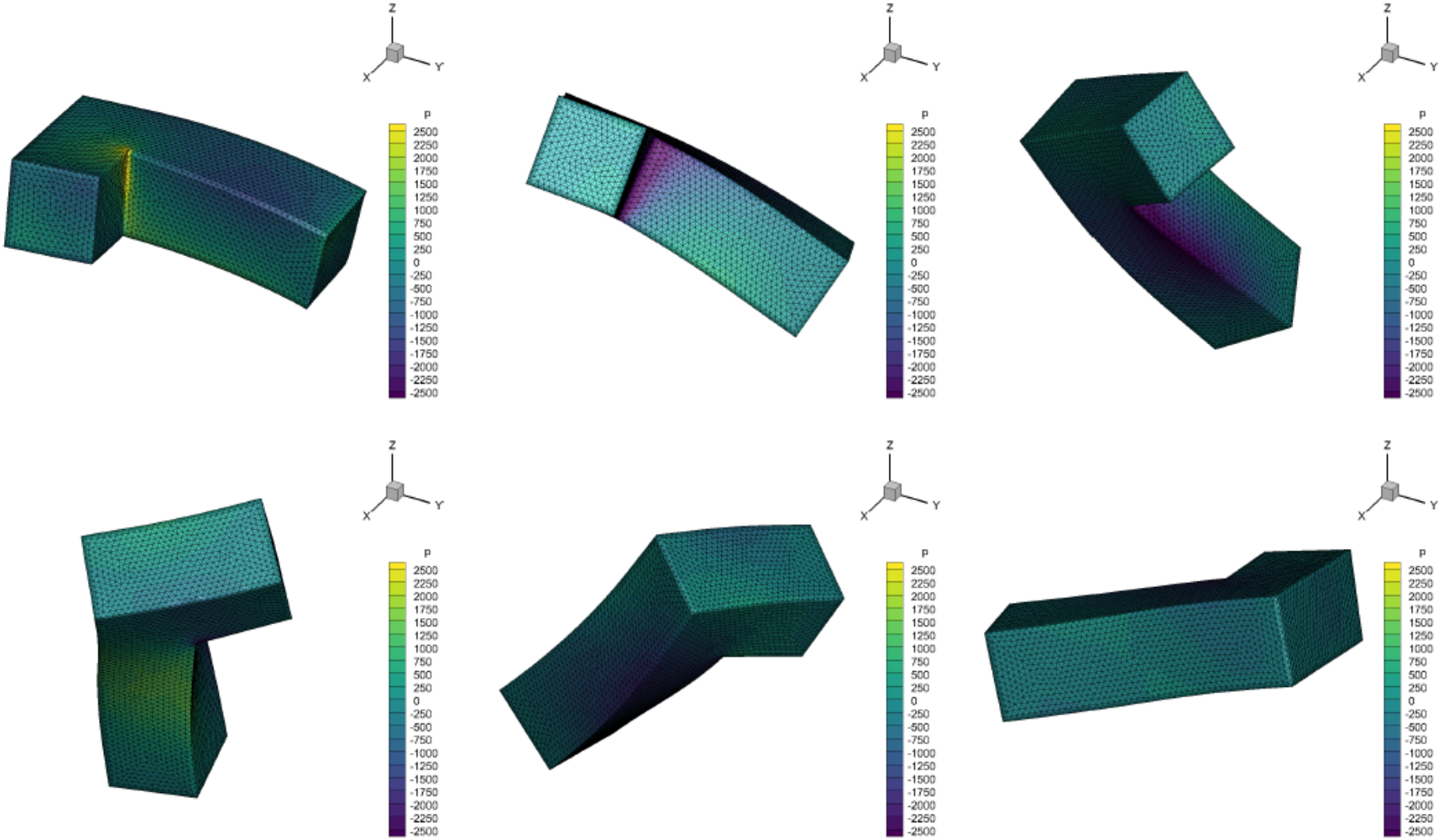

L-shaped problem – Angular momentum conservation

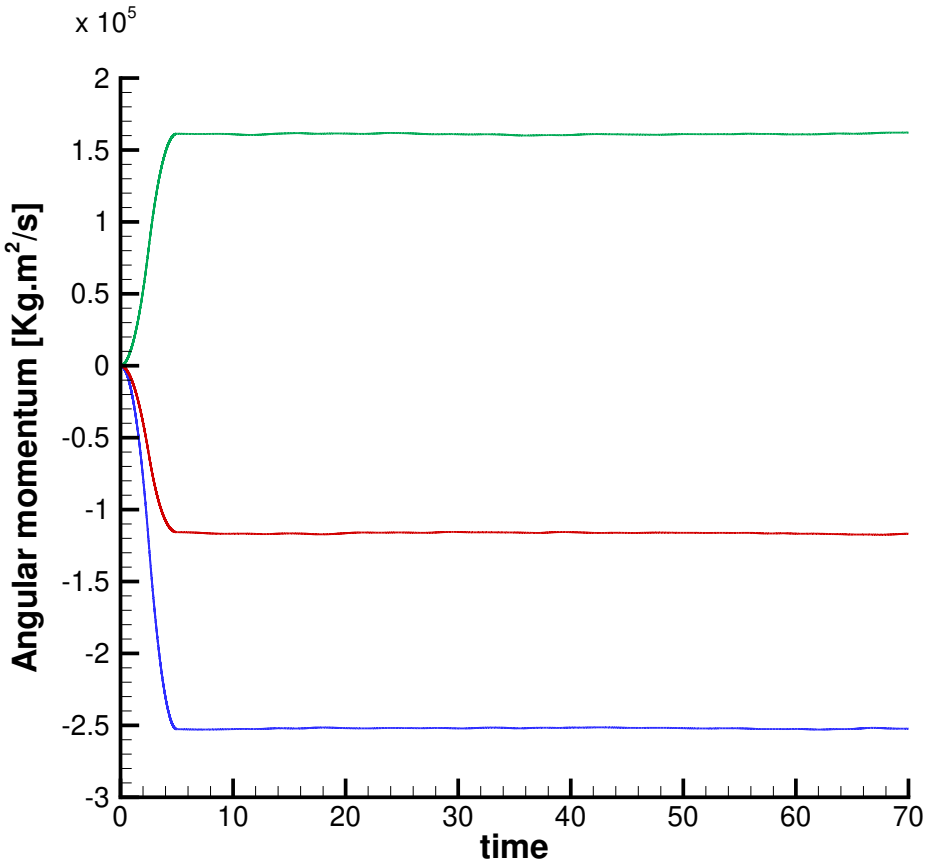

$$\begin{aligned} \boldsymbol{A} &= (A_x, A_y, A_z) = \\ &= \int_\omega \boldsymbol{x} \times m\,\boldsymbol{v}\,\mathrm{d}v \\ &\approx \sum_c \boldsymbol{x}_c \times m_c\,\boldsymbol{v}_c\,|\omega_c| = \boldsymbol{A}_c. \end{aligned}$$

Consistency relations $\epsilon_\omega = \big||\omega_c^{n+1}| - \tau_c^{n+1} m_c\big|$, $\epsilon_{\mathbb{B}} = \Big|\sqrt{\det \mathbb{B}_c^{n+1}} - \dfrac{\tau_c^0}{\tau_c^{n+1}}\Big|$.

Test case	Beryllium plate	Thick beam	Bar rebound	Blake	Jelly impact	Twisting column
$\max(\epsilon_{\mathbb{B}})$	5.86×10^{-13}	3.08×10^{-13}	1.12×10^{-12}	9.85×10^{-12}	4.19×10^{-12}	4.81×10^{-13}

Impact of a jelly-like droplet – Neo-Hookean vs NL models

[Hank et al., *JCP*, 2017]

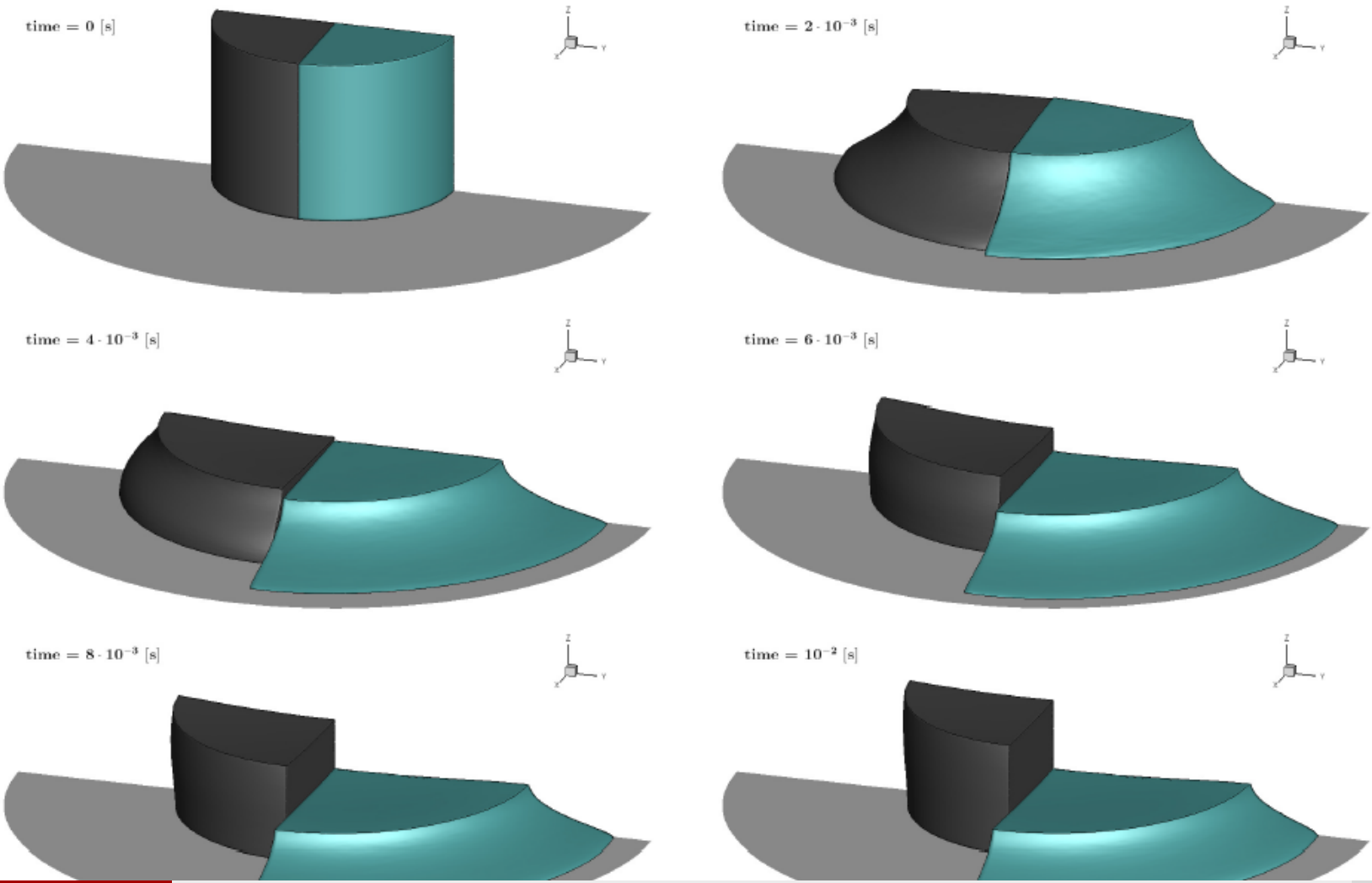

Impact of a jelly-like droplet – Neo-Hookean vs NL models

[Hank et al., *JCP*, 2017]

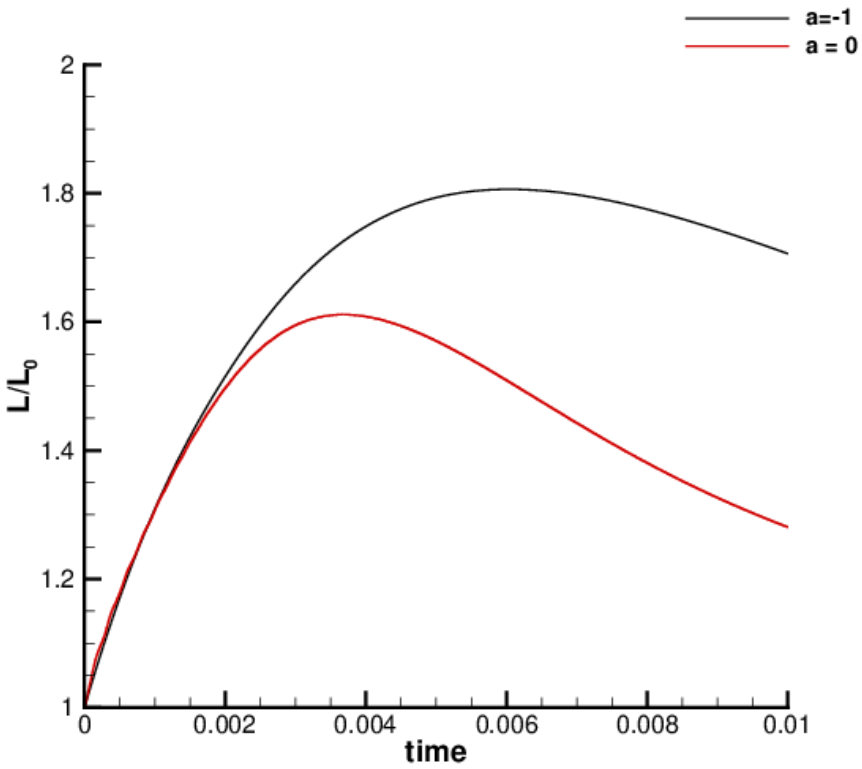

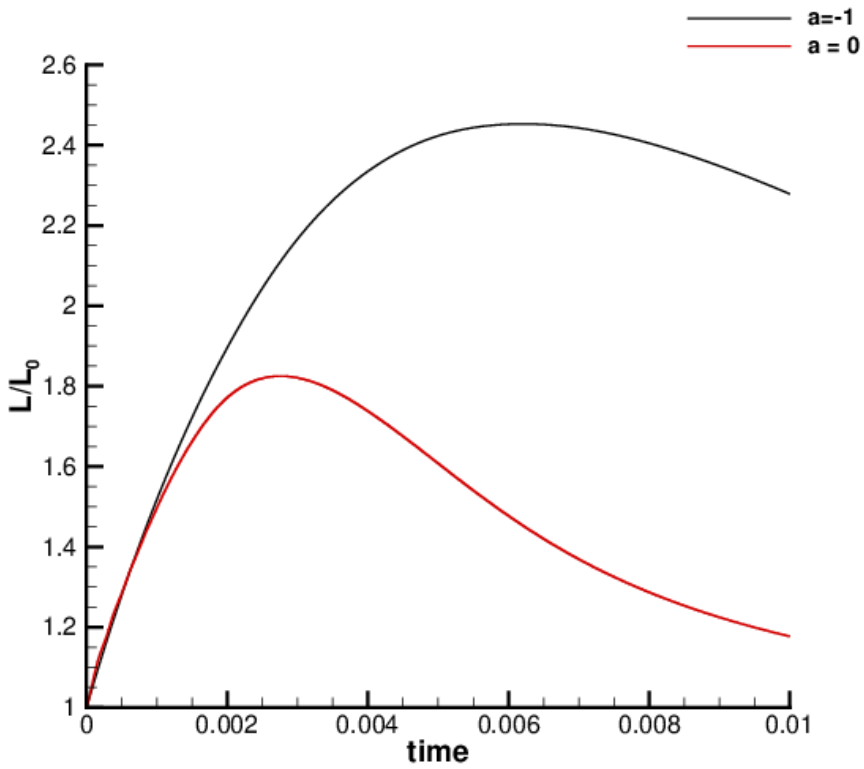

Time evolution of the maximum spreading of the droplet L/L_0 in the case neo-Hookean model ($a = -1$, black line) or non-linear one ($a = 0$, red line) The impact velocity is 2 m.s^{-1} (left) and 3 m.s^{-1} (right).

Outline

Conclusions and perspectives

We have presented a

- cell-centered Lagrangian finite volume schemes for hyperbolic system of PDEs (hydro and hyperelasticity);
- compatible GCL discretization on unstructured meshes in 2D/3D;
- second order of accuracy in space (MOOD) and in time (ADER);
- extended validation on benchmarks in gasdynamics and nearly incompressible solid mechanics.

We have **not** presented

- complete description of BCs, the underlying MPI parallelisation,
- exhausive description of the material properties (test cases),
- all hidden tricks.

Conclusions and perspectives

We have presented a

- cell-centered Lagrangian finite volume schemes for hyperbolic system of PDEs (hydro and hyperelasticity);
- compatible GCL discretization on unstructured meshes in 2D/3D;
- second order of accuracy in space (MOOD) and in time (ADER);
- extended validation on benchmarks in gasdynamics and nearly incompressible solid mechanics.

We have **not** presented

- complete description of BCs, the underlying MPI parallelisation,
- exhausive description of the material properties (test cases),
- all hidden tricks.

Perspectives

- plasticity effects;
- high order curvilinear finite volume schemes;
- extension to multi-material continuum mechanics.

Merci !
Merci vìelmol!
Thank you!

Works related to this presentation

[1] W. Boscheri, R. Loubère, P.H.-Maire. A 3D cell-centered ADER MOOD Finite Volume method for solving updated Lagrangian hyperelasticity on unstructured grids. *J. Comput. Physics*, Volume 449, 15 January 2022, arXiv:2104.02139.

[2] W. Boscheri, M. Dumbser, R. Loubère, P.H.-Maire. A second-order cell-centered Lagrangian ADER-MOOD finite volume scheme on multidimensional unstructured meshes for hydrodynamics. *J. Comput. Physics*, Volume 358, 2018, Pages 103-129

Conferences in 2022?

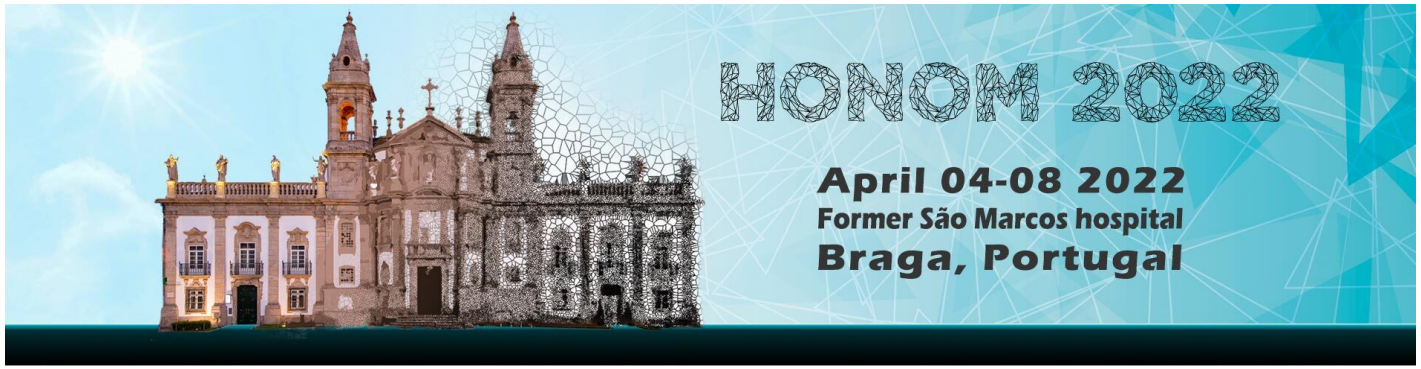

Braga, PT, HONOM 2022 `shark-fv.eu/honom2022/`

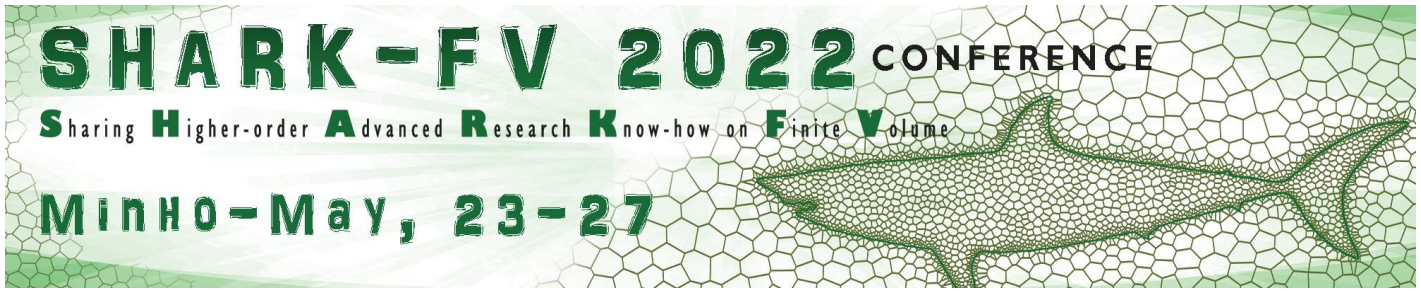

Povoa de Varzim, PR, SHARK 2022 `shark-fv.eu/home-shark/`

Malaga, Spain, HYP 2022 `hyp2022.com/cms.php`

Hyper-elasticity versus hypo-elasticity.

Hyperelasticity relies on the definition of a free energy which allows to express the deviatoric part of the Cauchy stress in terms of the deviatoric part of the left Cauchy-Green tensor. This framework provides a constitutive law fulfilling

- the material frame indifference principle;
- the thermodynamic consistency with the second law.

On the other hand, for hypo-elasticity, refer for instance to [47], the constitutive law is written under incremental form. Namely, the time rate of change of the deviatoric stress is expressed in terms of the deviatoric part of the strain rate tensor. The enforcement of the principle of material frame indifference relies on the use of a somewhat arbitrary objective stress rate such as the Jaumann rate, refer to [35]. Moreover, the use of objective stress rate makes appearing non conservative terms which render the mathematical analysis of discontinuous solutions quite delicate. This framework does not allow the fulfillment of thermodynamic consistency. Indeed, for smooth elastic flows the entropy is not conserved.